Conceptual model of the Tatun geothermal system, Taiwan

Patrick Dobson[a] Erika Gasperikova[a] Nicolas Spycher[a] Nathaniel J. Lindsey[a1] Tai Rong Guo[b] Wen Shan Chen[b] Chih Hsi Liu[b] Chun-Jao Wang[c] Shyh-Nan Chen[c] Andrew P.G. Fowler[d2]

Abstract

The Tatun geothermal system, located in northern Taiwan, is hosted by the Plio-Pleistocene Tatun volcanic group, consisting dominantly of andesitic lavas, domes and pyroclastic flows. During the late 1960s and early 1970s, geologic mapping, geochemical sampling, geophysical surveys, and the drilling of numerous exploration and temperature gradient wells were conducted at Tatun under the leadership of the Mineral Research and Service Organization (MRSO), the predecessor to the geothermal group at the Industrial Technology Research Institute (ITRI). Deep (1–2 km) wells encountered commercial temperatures (200–300 °C) in the Matsao area, but these initial exploration efforts were discouraged by the presence of very acidic (pH <3.5) and highly corrosive fluids. Numerous geoscience studies conducted over the past 15 years at Tatun have shown that the central portion of the system is dominated by corrosive volcanic fluids, as evidenced by abundant SO_2 as well as HCl. More reduced gases are encountered on the flanks of the system, suggesting that water-rock interaction may have at least partly neutralized the volcanic-derived fluids on the margins of this geothermal system.

Scientists from Lawrence Berkeley National Laboratory (LBNL) and ITRI have been working together to develop an updated evaluation of the Tatun geothermal system, with the goal of evaluating the geothermal resource potential of the NE margins of the Tatun geothermal system (Zone C), just outside of Yangmingshan National Park. This study provides a review and analysis of existing and new fluid geochemistry data, describes new magnetotelluric data and associated 3-D modeling conducted at LBNL, and incorporates these data and analyses with information from previous studies to create an updated conceptual model for the Tatun geothermal system, with a focus on the Zone C region. These data all suggest that the Zone C area is located on the margin of the main Tatun geothermal system. An exploration well drilled by ITRI will provide important constraints regarding the thermal regime and fluid compositions for this marginal portion of the system.

1. Introduction

The Tatun geothermal system is hosted in the Tatun Volcano Group, located in the northern part of Taiwan (Fig. 1). The area was seen as a promising target for geothermal exploration due to the abundance of hot springs and fumaroles associated with young volcanic rocks. The Mineral Research and Service Organization (MRSO) and the Chinese Petroleum Corporation (CPC) conducted extensive exploration efforts at Tatun from the late 1960s

until the early 1980s. This work included geologic mapping, geochemical sampling, geophysical surveys, and the drilling of more than 20 exploration wells (>500 m deep) and even more shallow (<500 m) temperature gradient wells (MRSO, 1969, MRSO, 1970a, MRSO, 1970b, MRSO, 1970a, MRSO, 1970b; Feng and Huang, 1970; Chen, 1970; Chen and Wu, 1971; Ellis, 1973; Lan et al., 1980; Chen and Yang, 1984). Five deep (570–1498 m) wells drilled by MRSO succeeded in encountering commercial temperatures (200–300 °C) in the Matsao area (Fig. 2), but encountered very acidic fluids that corroded the casing and well heads.

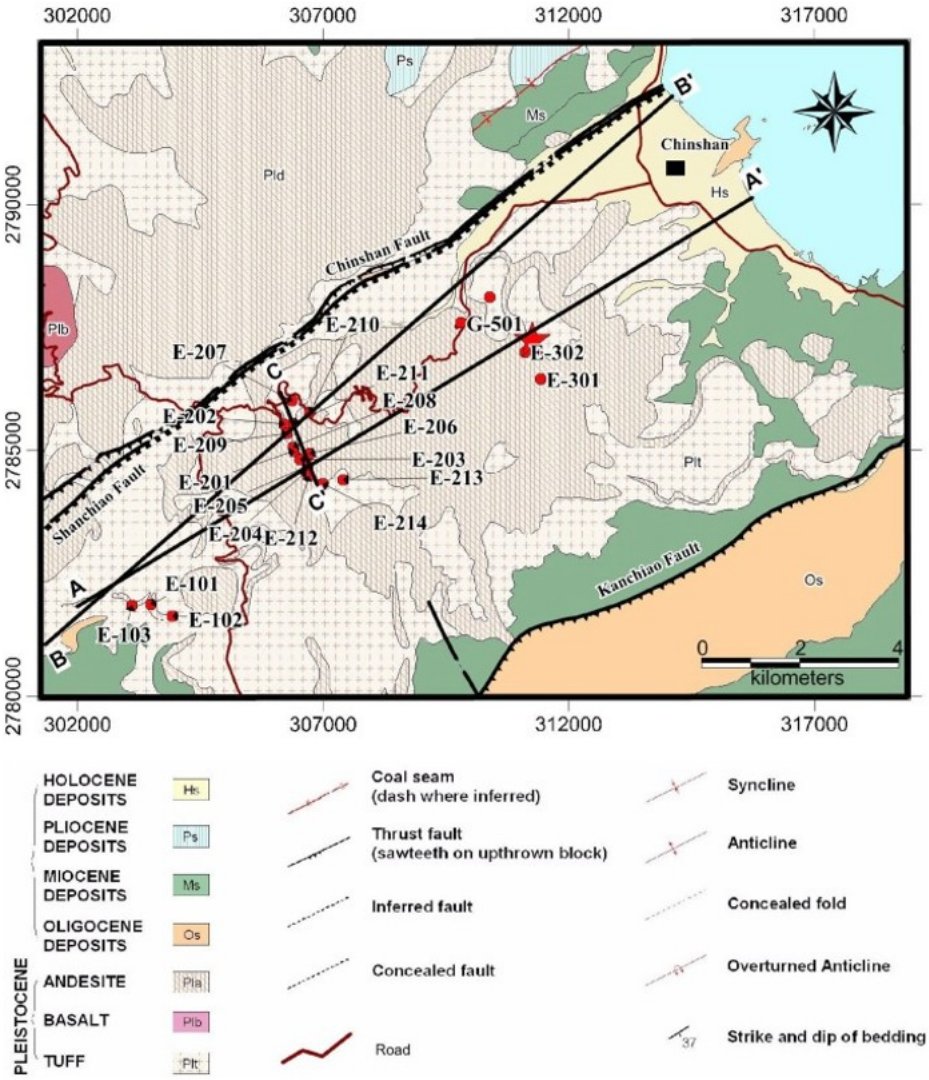

Fig. 1. Geologic map of the Tatun volcanic center, NE Taiwan. Red dots indicate the location of deep temperature gradient and exploration wells. Red star denotes the location of the ITRI exploration well in Zone C (the results of this well, drilled to assess the geothermal viability of this area, are not reported in this paper). Axis coordinates are in UTM (TWD97 datum, Zone 51R (North)) – northing and easting values are in m. Cross section A-A’ is depicted in Fig. 30, cross section B-B' in Fig. 27, and cross section C-C' in Fig. 2.

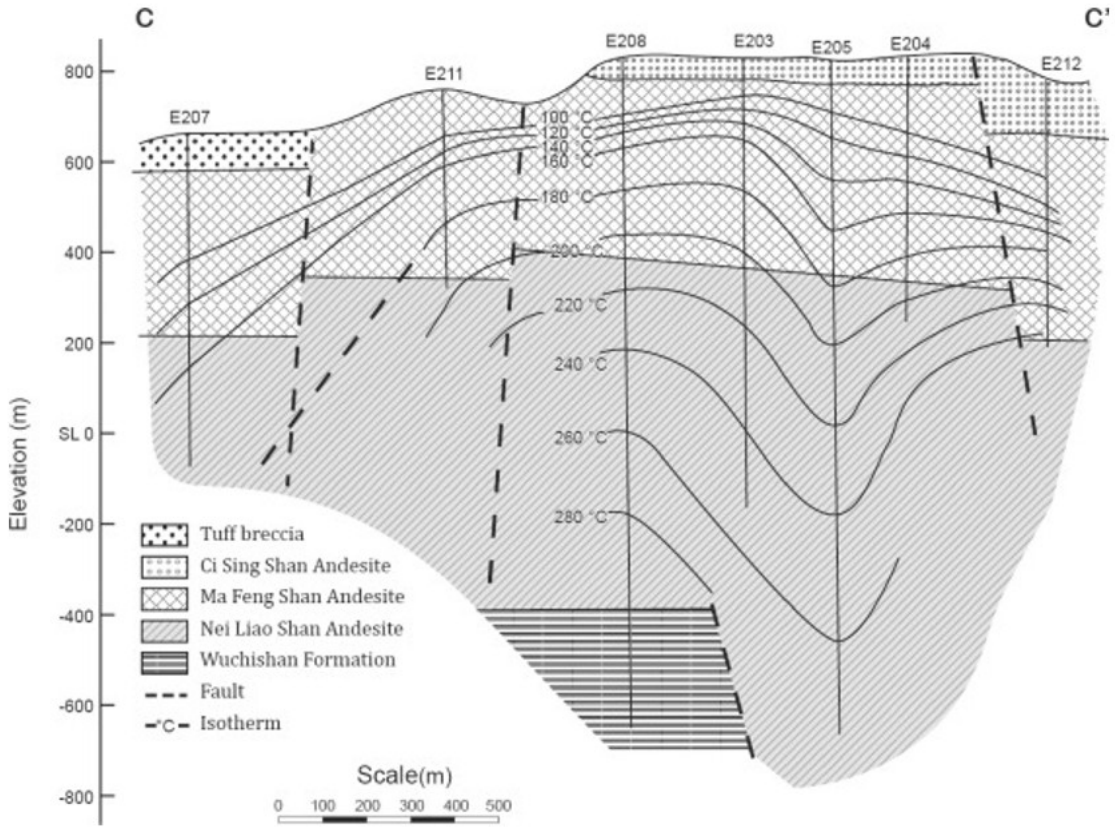

Fig. 2. NNW-SSE cross section through the Matsao area (see Fig. 1) depicting the stratigraphy and thermal structure of the Tatun geothermal system. Note that temperatures exceeding 290 °C were encountered in well E208 at depths less than 2 km.

Adapted from Lee et al. (1994).

Following the work conducted by MRSO, the CPC drilled three deep exploration wells. The CPC-MT-1T well was drilled in the Matsao area in 1981–1982 to a depth of 1717 m and encountered a sequence of volcanic lithologiesdown to a depth of 1626 m, where the sedimentary Wuchihshan Formation (Lower Miocene quartz sandstone) was encountered. This well encountered bottom-hole temperatures just above 200 °C. The corresponding alteration mineralogy for this well (with an assemblage of epidote, actinolite, and chlorite below 1100 m) appears to indicate temperatures that were hotter (~300 °C) than are currently encountered (Chen and Yang, 1984). The CPC-SHP-1T well, located near Szehuangtzeping, was drilled to a depth of 2 km (unpublished CPC report). This well only encountered temperatures slightly above 160 °C, suggesting that it marks the outer margin of the Tatun hydrothermal system. The CPC-CSN-1T well at Chinshan was drilled in 1980 to a depth of 2001 m (unpublished CPC report). This well encountered an upper (~70 m thick) interval of beach sands and terrace deposits that overlie a ~140 m thick section of the Muchan Formation (Lower Miocene sandstone/shale), followed by a very thick (>1500 m) section of the quartz-rich sandstone of the Wuchihshan Formation. The temperature in the CPC-CSN-1T well showed a reversal at a depth of around 300 m (with a

corresponding estimated local temperature maxima of ~103 °C), indicating the presence of outflow, and maximum values at total depth less than 150 °C.

These early studies confirmed that temperatures greater than 200 °C could be found in the central portion of the Tatun geothermal system at depths less than 2 km. However, severe corrosion issues that occurred with these wells raised the question of whether or not near-neutral fluids could be encountered in the deep reservoir. The recommendations of White and Truesdell (MRSO, 1970b) included the following suggestion:

“The most attractive possibility for geothermal resourcesmay be large reservoirs (2 sq. km or larger) in Miocene sandstones below the volcanic cover. The most important questions concern the depth of cover, the size and permeability of the reservoirs, and, especially, the primary acidity of the deep fluids. Our available evidence suggests that the primary acidity may be intolerably high (pH about 2?) especially near the fumarolic areas. If primary acidity is very high, we regretfully conclude that any deep resources are economically unattractive under present conditions. If, in contrast, the deep fluid is not too corrosive, we strongly urge a vigorous effort to discover large reservoirs by geophysical methods and deep drilling. If the deep water at Matsao is too acid by only a small margin, drilling further away from a fumarolic area may produce deep water with more of its primary acidity neutralized (1/2 to 1 pH unit higher), which may be acceptable for development.”

The objective of the present study is to reevaluate the viability of developing the Tatun geothermal system. Since the early drilling work was conducted at Tatun, much of the area has been transformed into the Yangmingshan National Park. Any new drilling must take place outside of the current park boundaries. While the central portion of the Tatun system appears to have fluids that are too acidic for commercial development, variations in gas geochemistryobserved in the fumaroles in the NE margins of the Tatun geothermal system (hereafter referred to as Zone C) appear to indicate a decrease in volcanic signature, with fluids that are more geothermal in character. This work provides an updated conceptual model of the Tatun system that examines the NE sector of Tatun as a possible exploration target.

2. Geology of the Tatun area

In order to develop a conceptual model for the Tatun geothermal system, it is critical to understand the geologic and tectonic framework of the area. The Tatun region has undergone a complex tectonic and structural history. Pliocene-Quaternary volcanism at Tatun is interpreted to be related to lithospheric extension in the N. Taiwan mountain belt, with the mantle source modified by subduction-related processes, and is not thought to be part of the Ryukyu volcanic arc (Wang et al., 1999). While most of Taiwan is currently undergoing crustal shortening, northern Taiwan is experiencing

extensional deformation. When the area was under compression, two major thrust faults were formed: the Kanchiao fault (east of Shihlin and Wanli), and the Chinshan fault (west of Peitou and Chinshan) (Chen, 1970). Coincident with the Chinshan thrust fault is the currently active Shanchiao normal fault, which strikes NNE with a dip of ~60° to the SE (Cheng et al., 2010). This feature appears to bound the geothermal activity at Tatun (Fig. 1), as all of the thermal features are located SE of this fault. Another structural feature, the Chilian lineament, appears to serve as the other bound to the geothermal area.

Initial studies of the volcanic history and stratigraphy of the Plio-Pleistocene Tatun Volcano Group (TVG) subdivided the TVG into three major subgroups (Chen, 1970) and further divided the area with geothermal activity into eight volcanic subgroups (Chen and Wu, 1971), noting that the Tatun system consisted dominantly of andesitic lavas, domes and pyroclastic flows. Song et al. (2000) conducted a detailed reevaluation of the Tatun volcanic center, and noted that it consists of around 20 volcanic centers (cones and domes) over an area of about 400 km^2. These have been subdivided into six subgroups: the Chutzeshan, Tatunshan, Chihshinshan, Neiliaoshan, Huangtsuishan, and the Tinghuohsiushan volcanic subgroups. These centers are in two spatial clusters: one along the Chinshan fault, and the other on an ENE to NE trend east of the Chinshan fault. The first two of these groups are located in the western part of the TVG, and are distributed along the Chinshan fault. The next three subgroups are distributed along an ENE to NE trend east of the Chinshan fault. These two clusters intersect at the Tatunshan volcano, forming a half amphitheater that opens to the NNE. The last subgroup is located in the far NE of the volcanic system.

The Tatun volcanic rocks consist of lava flows, pyroclastic breccias, surges, tuffs, lahars, and reworked volcaniclastic rocks. Lava flows outnumber explosive volcanic products, and very little tephra units are observed in surrounding sedimentary basins. More than 15 lava layers can be identified. Some of the thicker flows have developed columnar jointing, and in some cases, near horizontal platy jointing is present. The most common rock types are orthopyroxene-clinopyroxene and orthopyroxene-clinopyroxene-hornblende andesites. Pyroclastic breccias are commonly formed of andesitic lapilli and blocks with a matrix of fine crystals, glass, and lithic fragments, are monomict in composition. These breccias are usually found in incised valleys; tuffs also restricted in their exposures. Volcaniclastic deposits are widely distributed along the N, W, and S aprons of the volcanic group, and typically consist of lahar and fluvial deposits.

Tsai et al. (2010) used new digital terrain model (DTM) and LiDAR DTM maps to identify potential volcanic hazards for the Taipei metropolitan region, and concluded that the Chihsingshan Volcano subgroup, located in the SW portion of the TVG, is the youngest volcanic center at Tatun. It consists of four types of volcanic features based on the DTM images: 1) the Chihsingshan strato or composite volcano, the highest peak in the Tatun

area (1120 m), 2) the Shamaoshan dome and a hidden dome located between Chihsingshan and Chihkushan, 3) the Baiyunshan and Hsiaotsaoshan lava cones, located in the SE part of the Chihsingshan Volcano subgroup, and 4) the Chikushan scoria cone. Many small craters are linearly distributed along two NE-trending normal fault systems, which cut near the summit of Chihsingshan volcano. These craters are well preserved, which suggests that they are quite young. Most of the volcanic features consist of lava flows, with 20 different flows having been identified; their thicknesses range from a few meters up to 300 m. Dated lava flows range in age from 0.22 to 1.5 Ma, as summarized in Song et al. (2000).

Knowledge of the ages, frequency, and location of volcanic activity at Tatun is critical for understanding the role of magmatism as the heat source for the associated geothermal system and its contribution to the fluid geochemistry of the system. More recent studies of the TVG have revealed that the most recent volcanism at Tatun may be younger than previously thought based on earlier K-Ar and Ar-Ar age dating. Chen et al. (2010) and Belousov et al. (2010) reported ^{14}C dating of some of the younger units yielded ages ranging from 23 Ka to as young as 6 Ka. The last eruption at Mt. Cising (e.g., Chihsingshan) was interpreted to have occurred at around 13 Ka; this consisted of an initial pyroclastic eruption, followed by a lava flow, block and ash flow, and a lahar. This same unit was previously dated at 220 Ka using Ar-Ar, which seemed much too old given the lack of erosion. The young carbon ages suggests that the volcanic center should be considered to be still active. Some of the microseismicity in the Tatun area has been interpreted as indicative of volcanotectonic events because they correspond to a stress tensor different than the regional one and occur below the hydrothermally active Chihsinshan area at relatively shallow (<2.5 km) depths (Konstantinou et al., 2009).

The pre-volcanic sedimentary basement at Tatun is also important for the conceptual model, as these rocks form part of the geothermal reservoir section. This sedimentary sequence consists of Miocene and Pliocene units – comprised by the Wuchihshan, Mushan, Taliao, Shihti, Nankang, Wutu, Tapu, Erkuei, Chinshui, and Yuantuntze Formations (Chen, 1970; Yen et al., 1984). The Wuchihshan Formation is the oldest Miocene unit; it consists of well-consolidated sandstone interbedded with siltstone and shale, and has a thickness greater than 900 m. The sandstone is quartz-rich, and has porosities as high as 23%. This unit is thought to be the primary basement unit beneath the Tatun area. The Mushan Formation is about 600 m thick, and consists of sandstone, shale, and a few coal seams up to 0.3–0.6 m thick, with the sandstone having an average porosity of ~15%, and a maximum value of 25%. The Mushan sandstone is less well consolidated and finer grained than the Wuchihshan sandstone. The Taliao Formation is a sequence of marine sandstones, shales, and siltstones. It consists of three members, with thicknesses (from lower to upper) of 280, 60, and 160 m. The middle member is comprised by a massive calcareous

sandstone, with more shale in the lower member. This formation appears to have lower porosity (and permeability), and may be a poor reservoir rock. The Shihti Formation consists of two members, the lower (160 m thick) characterized by three white sandstone beds, and the upper (150–160 m thick) composed of alternating sandstones and shales, along with five coal beds. The Nankang Formation consists of three members: a lower member (180 m thick) with alternating sandstones and shales, a middle sandstone member (90–105 m thick), and an upper member consisting of three subunits: a 60 m thick lower subunit of interbedded shale, mudstone, and sandstone, a 110–140 m thick massive to thick-bedded sandstone, and an upper unit (220 m thick) of interbedded sandstone and shale. The Wutu and Tapu units may be equivalent to the Nanchuang Formation, consisting of a lower member of sandstone, shale and coal beds, a second member (90 m thick) of coarse grained sandstone, a third member (90 m thick) of sandstone with shale and silt interbeds, and an upper member of sandstone with interbeds of shale and siltstone. The Erkuei Formation (uppermost Miocene) is composed of alternating fine-grained sandstone and mudstone. The Chinshui is Pliocene in age and consists of shale. The Yuantuntze Formation consists of shaly sandstone and sandy shale. The most important of these units for the Tatun geothermal system is the quartz-rich sandstone of the Wuchihshan Formation.

3. Geochemistry of Tatun geothermal fluids

Thermal features at Tatun consist of acid-sulfate, near-neutral bicarbonate, and acid-sulfate-chloride hot springs as well as fumaroles (Liu et al., 2011). Fluid sources for the Tatun geothermal system include volcanic-derived components, as evidenced by the elevated He isotope ratios and the presence of SO_2 in the central fumaroles, as well as meteoric waters, as indicated by stable isotopeanalyses of geothermal waters (Yang et al., 1999; Lee et al., 2008; Liu et al., 2011; Ohsawa et al., 2013). A discussion of the water chemistry, gas chemistry, and fluid origins follows. The gas geochemistry of the fumaroles and bubbling hot springs is analyzed to identify regions with less magmatic chemistry that may serve as potentially more attractive drilling targets.

3.1. Spring water chemistry

The spring waters at Tatun can be divided into three groups: acid-sulfate, near-neutral bicarbonate, and acid-sulfate-chloride waters. The locations of the thermal features at Tatun are depicted on Fig. 3. Liu et al. (2011)associated the acid-sulfate waters (Type I) with the deep Wuchihshan sandstone formation, the near-neutral bicarbonate waters (Type II) with the andesitic volcanic terrane, and the acid-sulfate-chloride waters (Type III) with the shallow Wuchihshan Formation. Although these associations with rock types may generally hold for springs, the type of water is more directly related to ongoing physical and geochemical processes regardless of terrane, although it is expected that acid waters are

less likely to become buffered in the quartz-rich Wuchihshan sandstone than in andesitic rocks (Liu et al., 2011). Disproportionation of SO_2 gas and H_2S oxidation, possibly accompanied by HCl gas condensation, is expected to yield Type I waters. Heating of shallow meteoric waters by steam, and peripheral outflow of geothermal fluids unaffected by sulfidic gases would typically result in Type II waters. The mixing of thermal fluids with seawater or formation water provides a reasonable explanation for the high Cl content of Type III waters. However, the source of acidity for such waters away from volcanic centers (i.e., the Chinshan-Tapu area to the NE) is less clear.

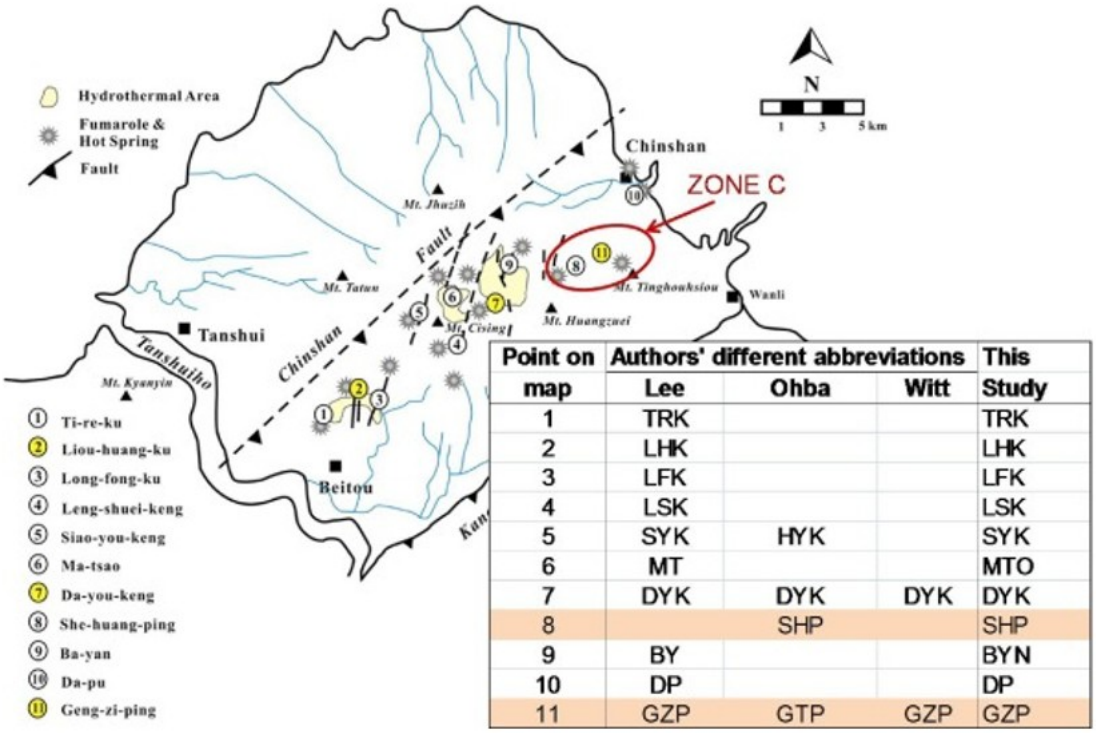

Point on map	Authors' different abbreviations: Lee	Ohba	Witt	This Study
1	TRK			TRK
2	LHK			LHK
3	LFK			LFK
4	LSK			LSK
5	SYK	HYK		SYK
6	MT			MTO
7	DYK	DYK	DYK	DYK
8		SHP		SHP
9	BY			BYN
10	DP			DP
11	GZP	GTP	GZP	GZP

Fig. 3. Locations of fumarolic and spring bubble gas analyses reported in the literature (Lee et al., 2005, Lee et al., 2008; Ohba et al., 2010; and Witt et al., 2008, at highlighted locations only). The table shows the different studies, location numbering and abbreviations used in this study. The map is adapted from Lee et al. (2005) and Witt et al. (2008). Zone C (features 8 & 11) is circled in red on the map, and related features are highlighted in the table because the focus of this study is to determine if this zone may serve as a potential commercial geothermal reservoir target.

The spring data from Liu et al. (2011) are shown in Fig. 4, Fig. 5. As shown on the $Cl/SO_4/HCO_3$ plot in Fig. 5, none of these waters can be considered “mature” geothermal waters, a term proposed by Giggenbach (1991) to define waters that have had time to reach some degree of equilibrium with reservoir rocks and that could be used for solute geothermometry analyses (Giggenbach, 1988). Most of the spring waters can be considered “immature” volcanic fluids, except for Type-II waters which fall in the fields of either steam-heated or peripheral (outflow) waters.

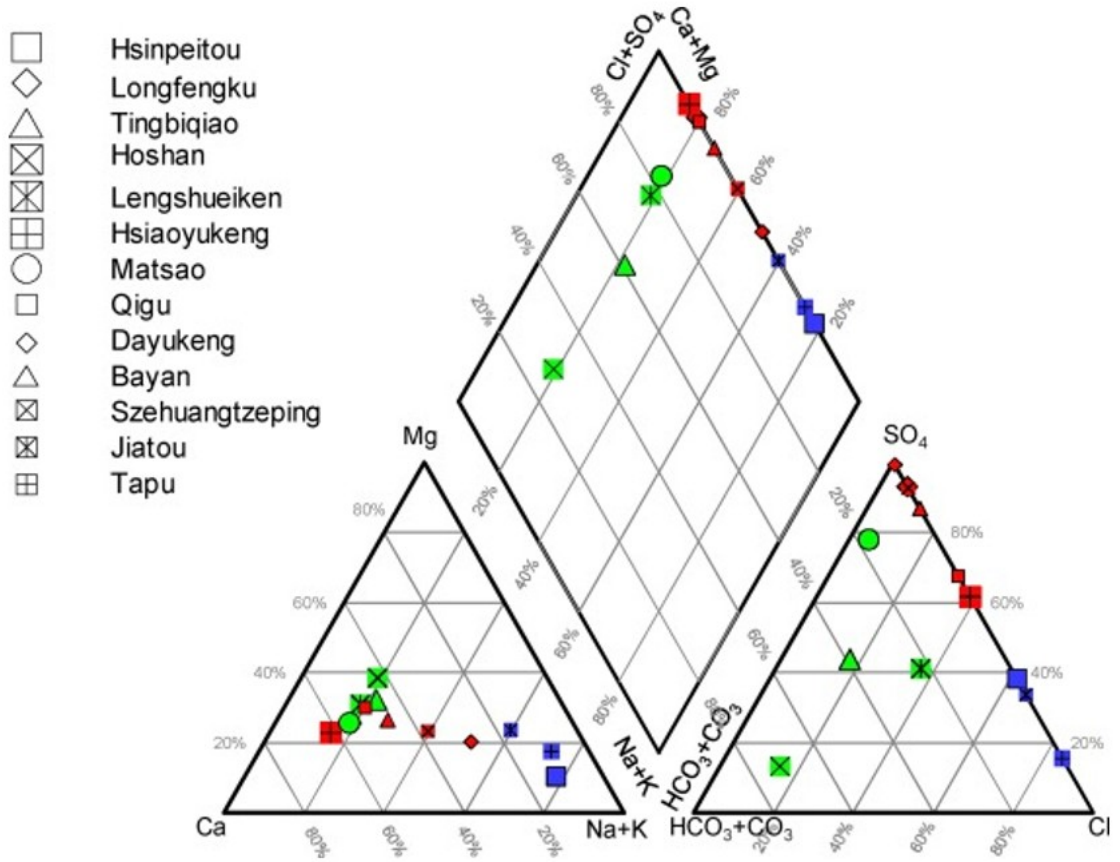

Fig. 4. Piper diagram showing the spring water analyses reported by Liu et al. (2011) in red: acid-sulfate; green: neutral-bicarbonate; blue: acid-chloride. Piper plot depicts data in meq%.

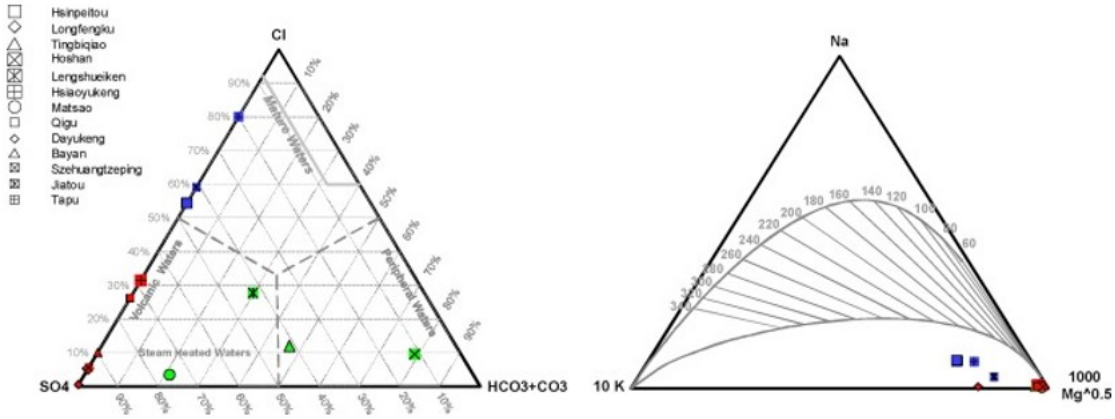

Fig. 5. Ternary diagrams for water classification (left) and Na-K-Mg geothermometry (right) showing the spring chemistry data of Liu et al. (2011) in red: acid-sulfate; green: neutral-bicarbonate; blue: acid-chloride. These plots depict data in ppm.

3.2. Subsurface water chemistry

ITRI compiled a list of water analyses from wells from old MRSO reports, mostly dating from 1967 to 1972, also including a few old spring analyses and data from more recent shallow monitoring wells (labeled starting with “TB-MW”). The location and numbering used in the present study for these

data points are shown in Fig. 6. A large proportion of these data are water analyses from the Matsao deep (1500 m) well E-205 (see Fig. 6), which are discussed in more detail because they represent the only available continuous record of deep water compositions at Tatun.

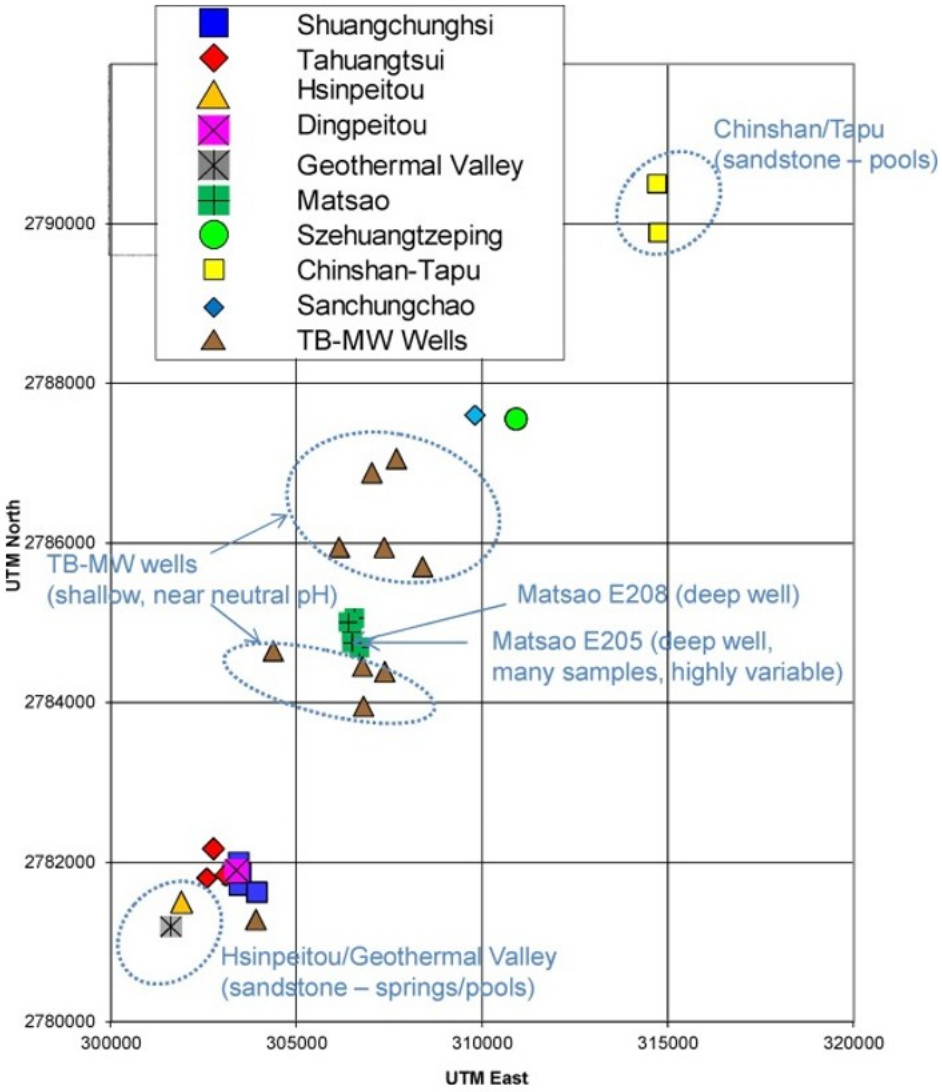

Fig. 6. Location of water samples (mostly from earlier wells) for which chemical analyses were compiled by ITRI for this study. Axis coordinates are in UTM (TWD97 datum) – northing and easting values are in m.

A review of these historical subsurface water compositions compiled by ITRI suggest that, similar to spring waters, most of these subsurface thermal waters reflect an immature volcanic character that is not suitable for geothermometry analysis. This is evidenced by the ternary plots shown in Fig. 7. One exception is some of the samples from deep (~1500 m) Matsao Well E-205, which fall on the edge of the “mature” field (Fig. 7, left), and form a clear linear trend, on the Na-K-Mg geothermometer ternary diagram

(Fig. 7, right), with an estimated Na-K temperature that corresponds closely with measured downhole temperatures (~260 °C).

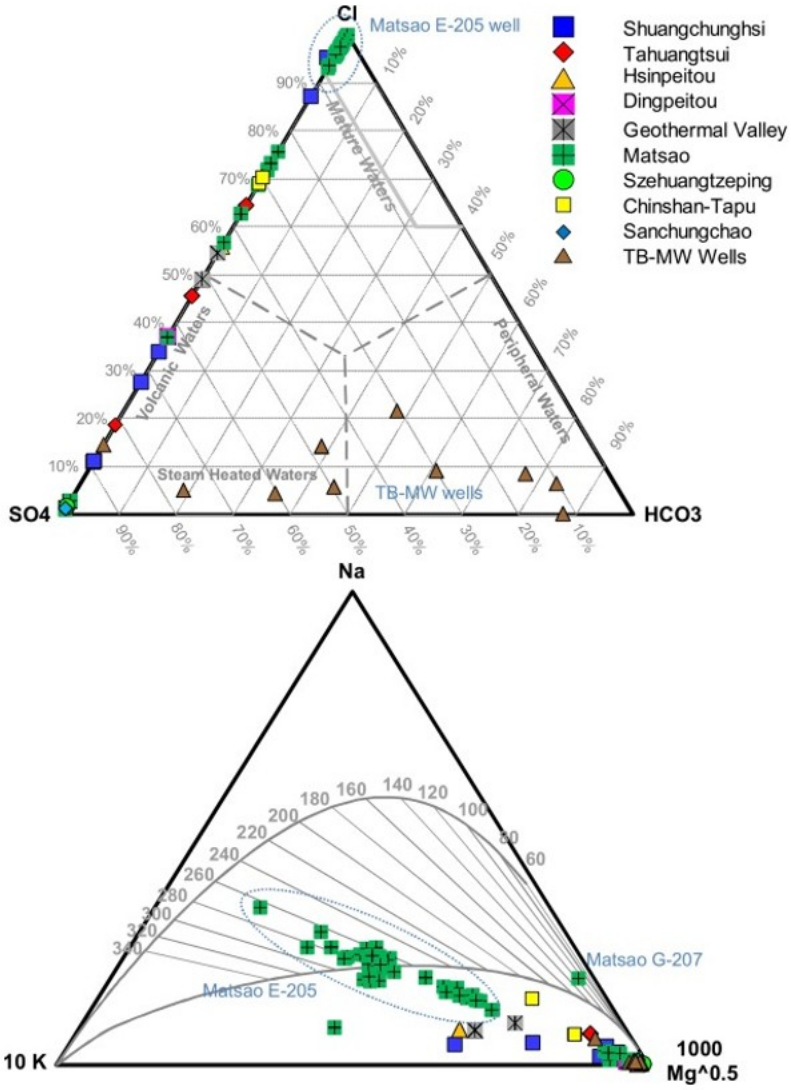

Fig. 7. Ternary diagrams for water classification (top) and Na-K-Mg geothermometry (bottom) showing the water chemistry data (from surface springs and wells) compiled by ITRI. Data are plotted in ppm.

Fluid samples from the deep exploration wells provide key insights into the potential presence of zones of non-acidic fluids in the deep geothermal reservoir. The early pH values reported from Matsao well E-205, from September to November 1969 fluctuated around 5 (MRSO, 1970a), which is near-neutral pH (~5.6) in the 200–300 °C temperature range. This suggests that more neutral, and potentially more mature fluids may have been present initially at depth at this location. However, it is unknown whether such fluids were widespread or not. Later data show that the pH remained mostly in the 4–5 range from November 1969 to November 1970, but then started to show significant variability, decreasing more often, at times to

values as low as 2 (Fig. 8). This might imply that the deep zone was invaded by acidic fluids, or that an acidic fluid entry within the wellbore started to dominate flow. Thus it is possible that a neutral zone initially dominated until pressure depletion, boiling or some combination of these factors caused production from an acid zone to dominate.

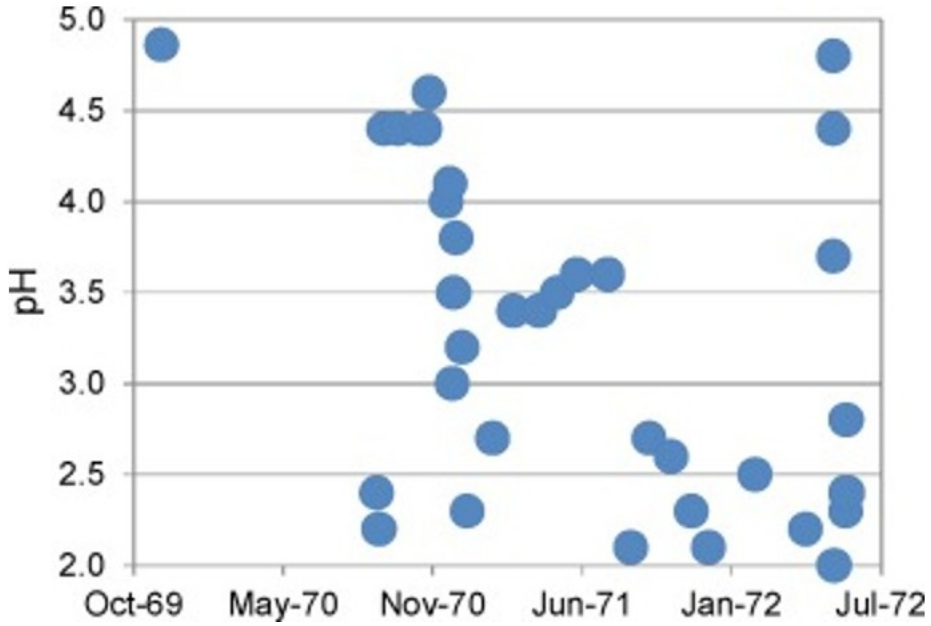

Fig. 8. pH data recorded for waters from Matsao well E-205 using data compiled by ITRI.

Chen, 1970, Chen, 1975 attempted to use the water samples from deep Matsao wells to infer the nature of deep fluids at Tatun. However, trying to infer the original reservoir fluid salinity from these data is difficult. The majority of the deep water samples from Matsao well E-205 show salinities around 22,000–50,000 mg/L, fluctuating at times to higher values that do not seem to correlate with the pH variations (compare Figs. 8 and 9). We suggest two plausible but very different interpretations. Na–Cl elemental correlation plots for these samples fall on an evaporation-dilution trend (Fig. 10), suggesting that the variable salinity could be caused in large part by boiling fluctuations through time (thus evaporative concentration fluctuations), starting with a fluid originally less concentrated than at later times after drilling. This would be supported by the fact that the first fluid sample from Matsao well E-205 recorded in ITRI's compilation (number 24, from November 1969) has a lower salinity (~14,000 mg/L) than samples collected at later dates. However, because this sample was collected sooner after drilling than the other samples, the possibility that it was diluted by drilling fluids cannot be ruled out. This in turn could explain why its composition plots off the trend of other E-205 samples on the Na-K-Mg ternary plot (Fig. 7). In contrast, the sample displaying the highest recorded salinity (number 27, October 1970, around 270,000 mg/L; Fig. 9, Fig. 10) is closest to the equilibrium line defined by the Na/K and K/Mg geothermometers on Fig. 7 (theoretically most "mature"), thus could instead be conceived as

representing the original fluid. If this was the case, the salinity decrease with time could be interpreted as the result of steam condensation from mixing of the original fluid with H_2O + acid gases liberated while drilling.

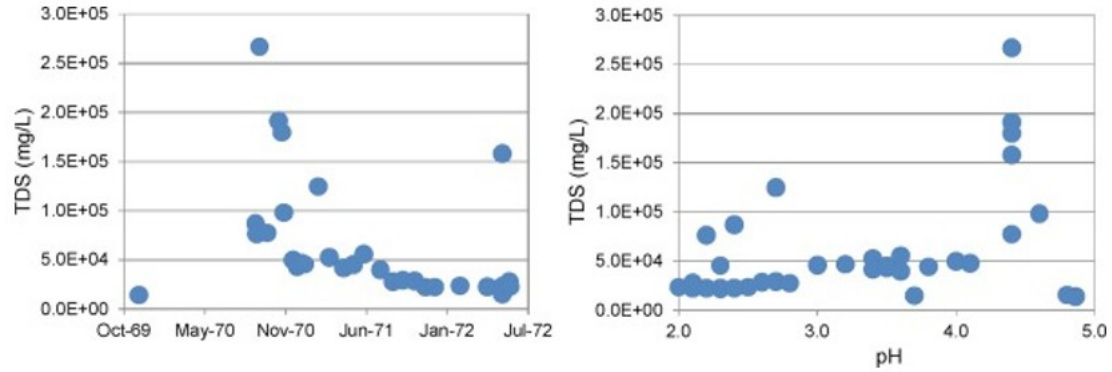

Fig. 9. Total dissolved solids (TDS) and pH of samples collected in Matsao deep (1500 m) well E-205 between 1969 and 1972.

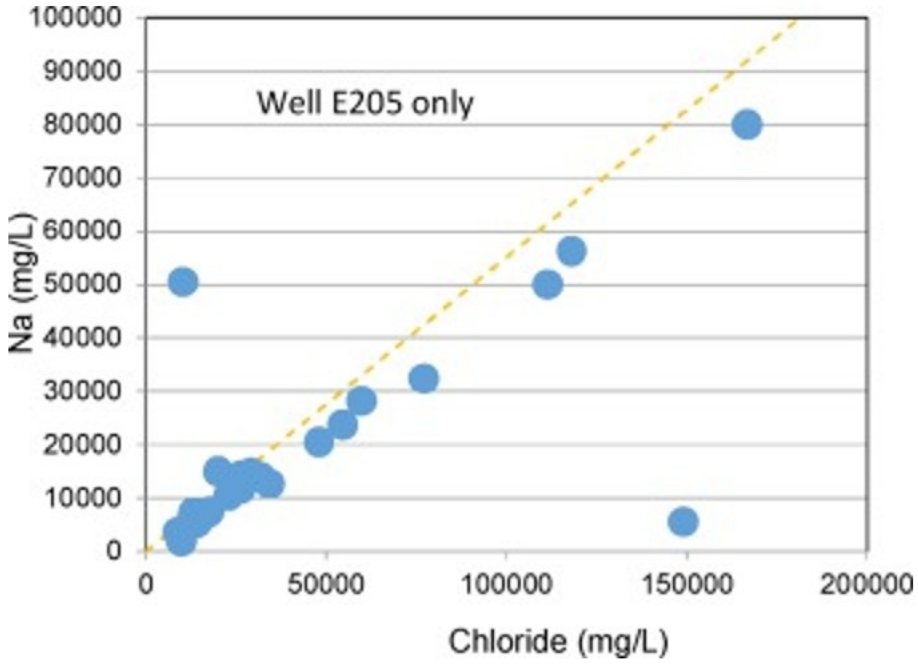

Fig. 10. Correlation plot of Na versus Cl for samples from Matsao deep well E-205. The dashed line follows the Na/Cl ratio in seawater.

Which of the above two interpretations holds best is unclear. Except for a mention of up to 80% steam discharge from this well (Feng and Huang, 1970), the sampling wellhead pressure was not available and thus steam/water ratios are unknown for the reported water analyses. Therefore, it is difficult to make firm conclusions about the salinity of the deep sampled fluids, except that highly saline samples are likely to have been concentrated by evaporation/boiling, and early, more dilute, samples may have been diluted by drilling fluids.

The fact that the majority of deep water samples in the Matsao area evolved to display a quite acidic character, in addition to elevated salinity, led early investigators to hypothesize the existence of a deep (Type-III like) fluid at Tatun, which was interpreted to result from a lack of neutralization of magmatic fluids containing SO_2 and HCl (e.g., White and Truesdell in MRSO, 1970b; Truesdell et al., 1989; D'Amore et al., 1999; Truesdell, 1991, Truesdell, 2000). Such a conceptualization, including the distribution of different water types, is illustrated in Fig. 11.

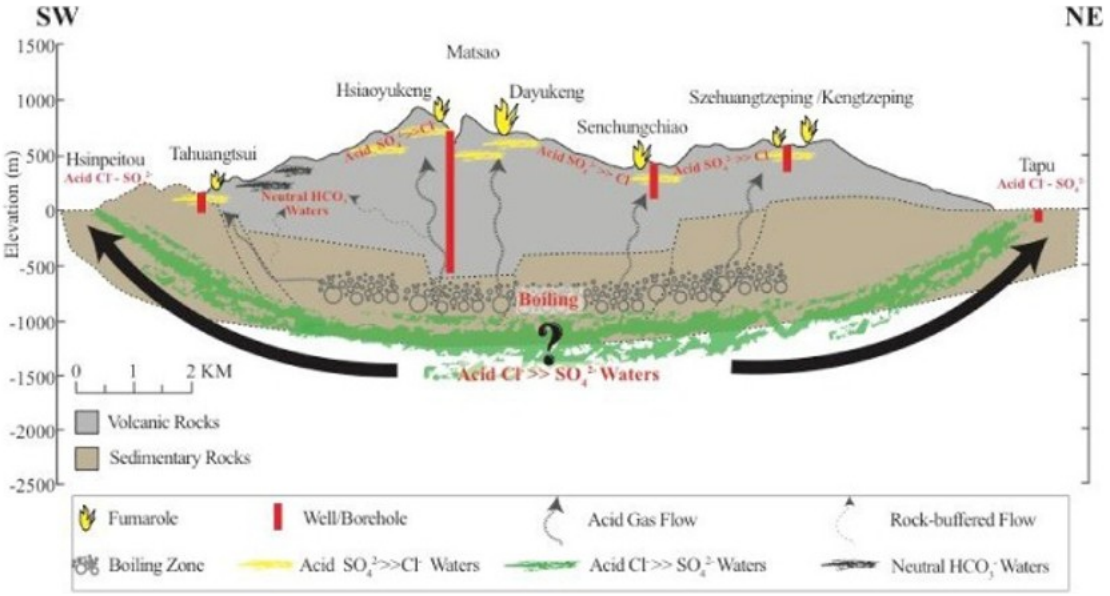

Fig. 11. Sketch of previously hypothesized geochemical conceptual model of a liquid-dominated acid-chloride system at depth at Tatun. This model does not appear consistent with the presence of calcite observed in deep Matsao wells.

However, such a conceptualization does not appear consistent with the deep alteration mineralogy reported in Matsao wells by Lan et al. (1980) and Chen and Yang (1984). Lan et al. (1980) reported three main alteration zones in these wells. Zone 1, at depths above 200 m, contains kaolinite, alunite, pyrite, and gypsum, and thus is typical of acid-sulfate alteration. In this zone, the original andesite textures are totally obscured and primary minerals completely replaced. In Zone 2, at depths between 200 and 500 m, a sporadic occurrence of laumontite, analcime, and hematite is reported, but smectite-chlorite, anhydrite, quartz, carbonate, and pyrite are abundant. Alunite, wairakite, type-III chlorite, and secondary albite are absent from this zone. The primary textures of the andesitic rocks in this zone are generally well preserved. Zone 3, at depths below 500 m, is characterized by the presence of epidote, wairakite, chlorite, albite, anhydrite, illite, quartz, and pyrite. This assemblage is typical of propylitic alteration and not consistent with acidic conditions at depth. Petrographic examinations of deep core samples from the E208 well (Fig. 12) did not find any sign of kaolinite or sulfates that might be expected to have formed by interaction with low pH fluids (MRSO, 1973a, MRSO, 1973b). Chen

and Yang (1984) reported three similar alteration zones for the CPC well at Matsao: an upper argillaceous zone, an intermediate chlorite zone, and a deep epidote-actinolite zone. They also reported calcite present in all three zones. These volcanic rocks also contain abundant feldspars, which would improve their capacity to buffer acidic fluids relative to the quartz-rich sandstones of the underlying Wuchihshan Formation. Therefore, the propylitic alteration (as opposed to acid alteration) and the presence of minerals with high neutralizing capacity such as feldspars and calcite, which would have fully dissolved under strong acid alteration, support the argument for the presence (at least initially) of neutral fluids at depth at this location. The lack of permeability in these rocks suggested by the conductive temperature gradient in Fig. 2 would further support this argument.

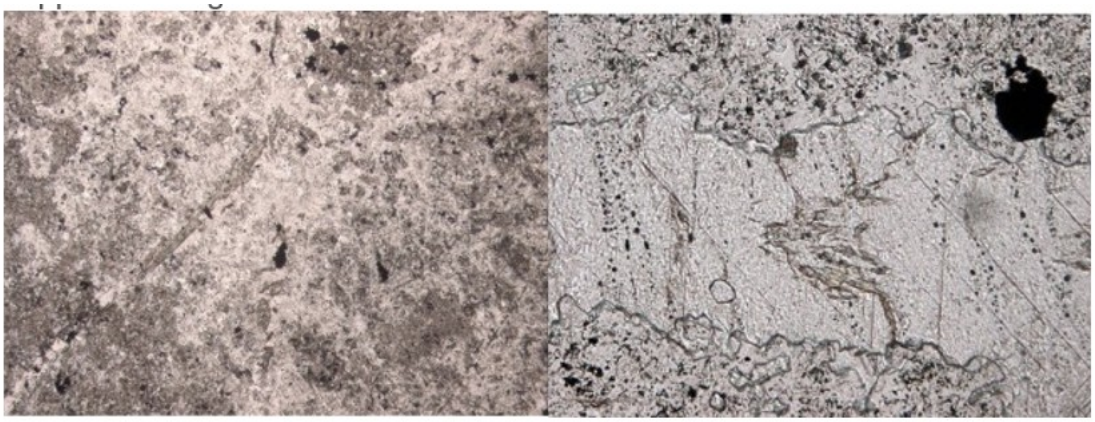

Fig. 12. Photomicrographs of hydrothermally altered andesitefrom E208 well at a depth of 1385 m (sample P39760). Alteration assemblage includes chlorite, epidote, quartz, adularia and chlorite (MSRO, 1973b). Image on left (uncrossed nicols) has field of view of 8 mm, close-up image on right of calcite vein (uncrossed nicols) has field of view of 500 μm. Photomicrographs and petrographic descriptions courtesy of Dr. Nick Mortimer, GNS Science.

3.3. Origin of acidic fluids

Fournier and Thompson (1993) showed that the hydrolysisof NaCl in high-temperature/low-pressure brine-steam systems (>350 °C) can generate HCl according to the reaction

(1)$NaCl_{(s)} + H_2O \rightarrow NaOH_{(s)} + HCl_{(g)}$

with NaOH eventually diffusing as a solid solution into NaCl. These authors also observed that the presence of quartz increased the production of HCl through the formation of sodium disilicate

(2)$4NaOH_{(s)} + 2SiO_2 \rightarrow Na_4Si_2O_{6(s)} + 2H_2O$

resulting in the overall reaction

(3)$4NaCl_{(s)} + 2H_2O + 2SiO_2(s) \rightarrow Na_4Si_2O_{6(s)} + 4HCl_{(g)}$

The HCl gas produced in this manner is extremely hydrophilic and thus dissolves into any water present to produce acidity

(4)$HCl_{(g)} \rightarrow H^+ + Cl^-$

Although such a NaCl hydrolysis mechanism requires temperatures above about 350 °C, it has been shown that other brines, such as $CaCl_2$ brines, can generate HCl at much lower temperatures (e.g., Zhang et al., 2009). D'Amore et al. (1999) have also shown that significant HCl gas concentrations can develop over brines with elevated Cl concentrations derived from boiling. Their thermodynamic calculations show, for example, that a 100,000 ppm_w Cl brine of pH 5 would equilibrate with about 10 ppm_w HCl in the gas phase at 250 °C, and 3000 ppm_wHCl at 350 °C.

Earlier studies at Tatun (e.g., White and Truesdell in MRSO (1970b), Truesdell, (1991)) have proposed the existence of a deep acidic fluid caused by HCl from NaCl hydrolysis at depth. The main rationale for this hypothesis was that the chloride concentrations measured in some of the water samples from the deep Matsao wells exceed the sum of concentrations of other cations (on an equivalent basis). Our review suggests that while this is sometimes the case, the fluid analyses may not be reliable enough to unequivocally conclude that samples from deep Matsao wells display excess chloride. Indeed, a significant charge imbalance is found for many of the analyses of water samples from these wells. The excess chloride concentrations correlate remarkably well with this imbalance (Fig. 13) rather than with pH (even when correcting the measured H^+ activity to actual concentrations).

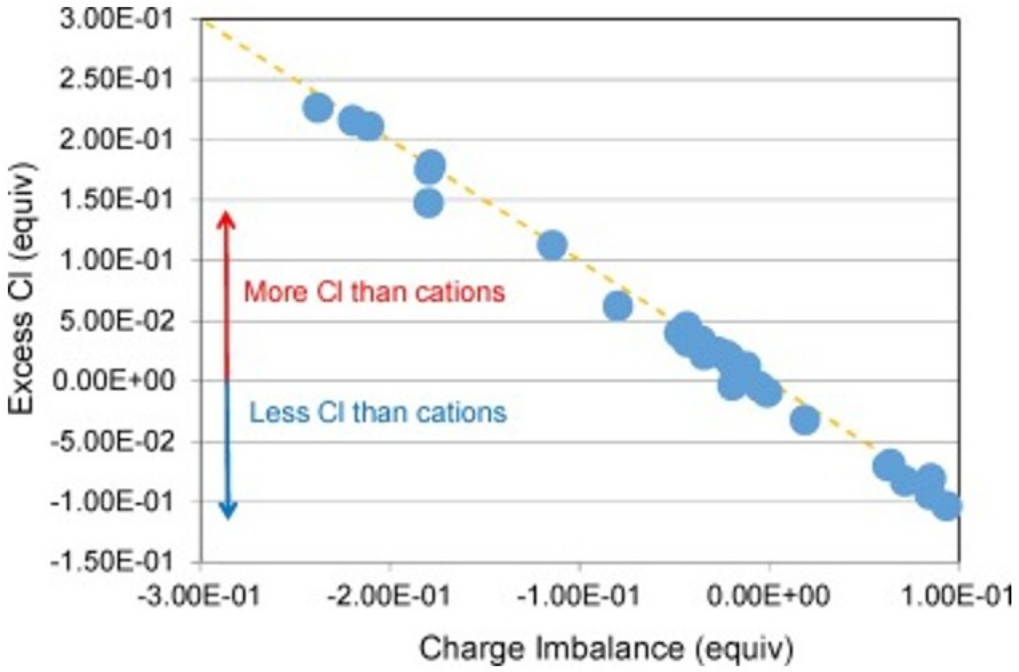

Fig. 13. Correlation between excess chloride and charge imbalance for water samples collected from Matsao well E-205.

For this reason, it would appear more probable that the acidity results primarily from the interaction of sulfidic gases (H_2S and SO_4) with deep, more neutral solutions, with Cl possibly originating from formation waters in the

Wuchihshan sandstone (Liu et al., 2011). The disproportionation of magmatic SO_2 gas produces acidity

(5) $4SO_{2(g)} + 4H_2O \rightarrow H_2S_{(g/aq)} + 3SO_4^{-2} + 6H^+$

which, closer to the surface is exacerbated by the oxidation of H_2S by atmospheric O_2

(6) $H_2S_{(g/aq)} + 2\ O_{2(g/aq)} \rightarrow SO_4^{-2} + 2H^+$

A plot of H^+ molality versus SO_4 molality for the Matsao well E-205 waters (Fig. 14, top) shows that waters in this well evolve toward the theoretical lines that would be expected if the all the acidity came from sulfuric acid. The fact that the majority of the samples plot near or below these lines strongly suggests that most of the acidity is related to sulfidic gases rather than HCl, which is also consistent with a review of gas analyses presented later in this report. Small quantities of HCl from boiling (to near-dryness) at depth and higher concentrations from magmatic sources near volcanic centers are not ruled out, however.

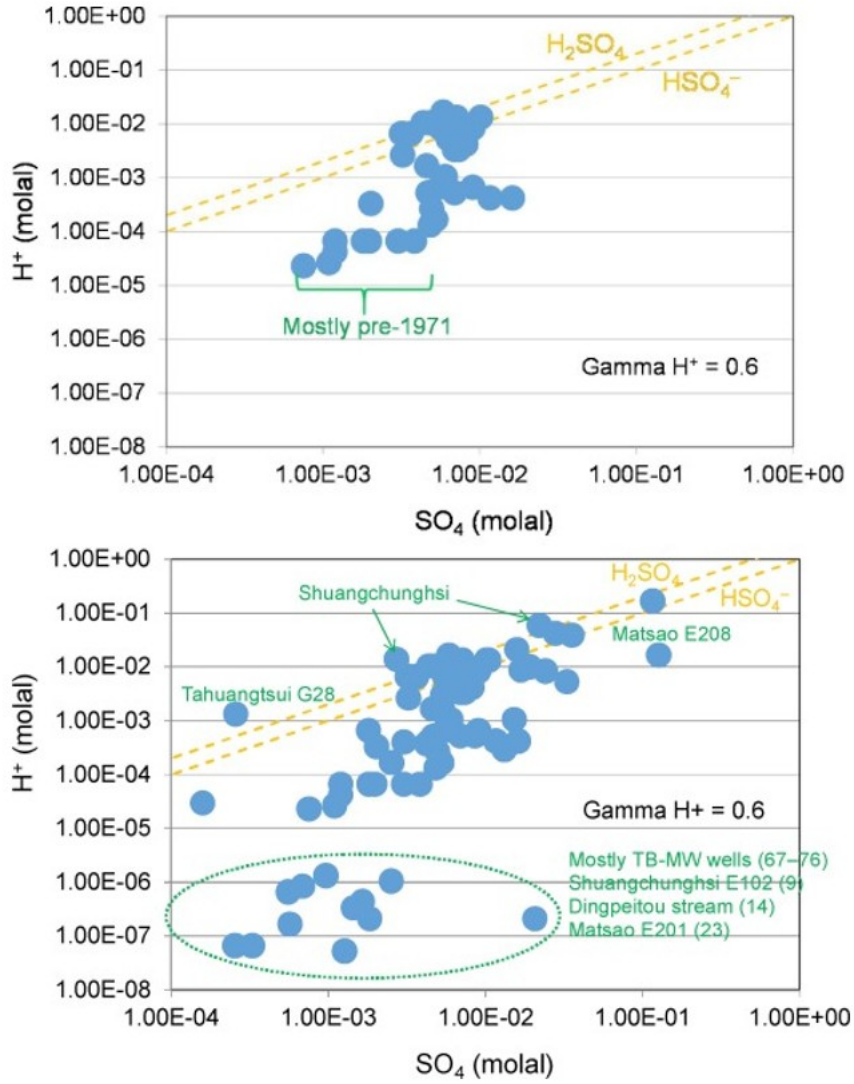

Fig. 14. Correlation between H^+ and SO_4 molality in the Matsao well E-205 waters (top) and other waters (bottom) compiled by ITRI. The dashed lines show the 1:2 and 1:1 slopes that would be expected from deprotonation of pure H_2SO_4. The H^+ molality is calculated from pH using an activity coefficient of 0.6 estimated for saline waters (the lines shift up slightly with higher activity coefficients).

Native sulfur is known to form by the reaction of H_2S and SO_2 as follows

$$(7) 2H_2S_{(g)} + SO_{2(s)} \rightarrow 3S_{(s)} + 2H_2O$$

resulting in sulfur deposits typically associated with fumarolic activity (solfataras). Such deposits are widespread at Tatun, and in some places have accumulated to economic quantities (e.g., the old sulfur mine at Genzinping – see feature 11 in Fig. 3). When groundwater interacts with such deposits, the hydrolysis of native sulfur is another process that yields significant acidity, without the need for added oxygen

$$(8) 4S_{(s)} + 4H_2O \rightarrow 3H_2S_{(aq)} + SO_4^{-2} + 2H^+$$

Such a process is likely also important in generating shallow acidic waters at Tatun in areas where older, buried solfataras exist, representing significant amounts of sulfur that has been deposited. However, the mineralogical evidence from deep Matsao wells make these models unlikely in the deep andesite at Tatun.

Old records of activities at Matsao (MRSO, 1971) show that in the Matsao deep well E205, decreasing pH values may have coincided with a decrease in flowing pressure, presumably due to blockage at depth. Vidal (1999) reports that blockage at depth in a production well at Balas-balas in the Philippines likely coincided with a decrease in the pH of the produced water. These authors observed a trend of increased discharge enthalpy with decreasing pH, together with lower flow rates at that well. They attributed these observations to the discharge (from shallow vapor-dominated zones) of acidic vapor into the shallower parts of the well (forming mostly H_2SO_4 in the produced fluids), which became proportionally larger than the liquid feed from deeper zones after blockage at depth. Because of the scarcity of operational records for these wells, including casing surveys, one cannot ascertain that the same mechanisms resulted in the observed pH drop in the deep Matsao wells. However, it is certainly a possibility that should not be overlooked.

3.4. Gas geochemistry

Fumarolic and spring gas compositions reported in the recent literature (Lee et al., 2005, Lee et al., 2008; Ohba et al., 2010; Witt et al., 2008) and additional data compiled and collected by ITRI for wells and a few springs were reviewed. Our primary objective was to investigate the variation of gas compositions in space and time as indicators of gas origin (i.e., volcanic versus geothermal/hydrothermal), cause of acidity (i.e., HCl versus sulfidic gases), and temperature through geothermometry analyses. The locations of the various gas datasets reviewed are shown on Fig. 3. These data are briefly discussed below, and additional details on the interpretation of these data can be found in the original studies.

All of the Tatun gas sampling surveys analyzed a suite of gases typical for studies of volcano-hosted geothermal systems, including Ar, N_2, CH_4, C_2H_6, He, H_2, O_2, HCl, H_2S, SO_2, CO_2, and H_2O. From 2003 to 2006, Lee et al., 2005, Lee et al., 2008 sampled these gases plus CO in an extensive survey of fumaroles and spring gases at Tatun along the entire SW-NE trend of thermal manifestations from Beitou to Chinshan (Fig. 3). Their interpretations of gas chemistry focused on the origin of the gas, especially in terms of magmatic and meteoric affinity, and reasons for the compositional variations with respect to time and location. Ohba et al. (2010) complemented the Lee et al. study with more spatially limited sampling of fumaroles in two areas (Fig. 3), reporting the basic suite and adding ^{4}He, ^{20}Ne, ^{36}Ar, ^{40}Ar, ^{84}Kr, and ^{132}Xe isotopes to support similar conclusions. Witt et al. (2008) sampled in two areas (Fig. 3), adding CO and Hg to the basic set of gases in a study

comparing conventional (Giggenbach, 1991) gas sampling to field-based gas analyzer techniques.

We also included in our review gas compositions compiled by ITRI. These data include analyses found in older reports for gas samples collected between 1967 and 1972, mostly in wells. The ITRI dataset includes analyses for CO_2, H_2S, SO_2, and O_2 and only four points with N_2, CH_4, and H_2 (for Matsao well E-205). This dataset has been supplemented with gas samples collected by ITRI between May 8th and October 8th 2015 at Geng-zi-ping (GTP or GZP) and She-huang-ping (SHP).

The data from all these sources were compiled into a database and subjected to various graphical analyses involving ternary compositional plots as follows (Fig. 15, Fig. 16, Fig. 17, Fig. 18, Fig. 19):

• N_2-He-Ar (Giggenbach, 1992) – This plot (Fig. 15) is useful to differentiate meteoric, magmatic, and crustal gas components, and type of magmatism and tectonism (e.g., basaltic vs. andesitic, subduction vs. continental). This type of plot also supplements He isotopic data that are used to differentiate between crustal (<0.1 R_A) and magmatic/mantle (>4 R_A) components, and has been shown to provide useful information for Tatun gases (Lee et al., 2005, Lee et al., 2008).

• N_2-Ar-CO_2 (Giggenbach, 1992) – This plot (Fig. 16) supplements the N_2-He-Ar plots to differentiate gas origins. For example, Giggenbach (1992) reports that the CO_2/N_2 ratio in the crust is ~200, and that this represents an intermediate value between ~2000 in the mantle and ~40 in subducted gases. Also, excess CO_2 in gas relative to N_2 and Ar may indicate CO_2 originating from subducted sediments.

• Other ternary diagrams are also useful to “fingerprint” gas types and origins. For example, the CO_2/S/HCl plot (Fig. 19) is useful to distinguish between more volcanic and hydrothermal/geothermal components (e.g., Lee et al., 2005, Lee et al., 2008), and a plot of CO_2/CH_4/S (Fig. 18) can provide information on the gas redox character, with high methane concentrations suggesting a more reduced character.

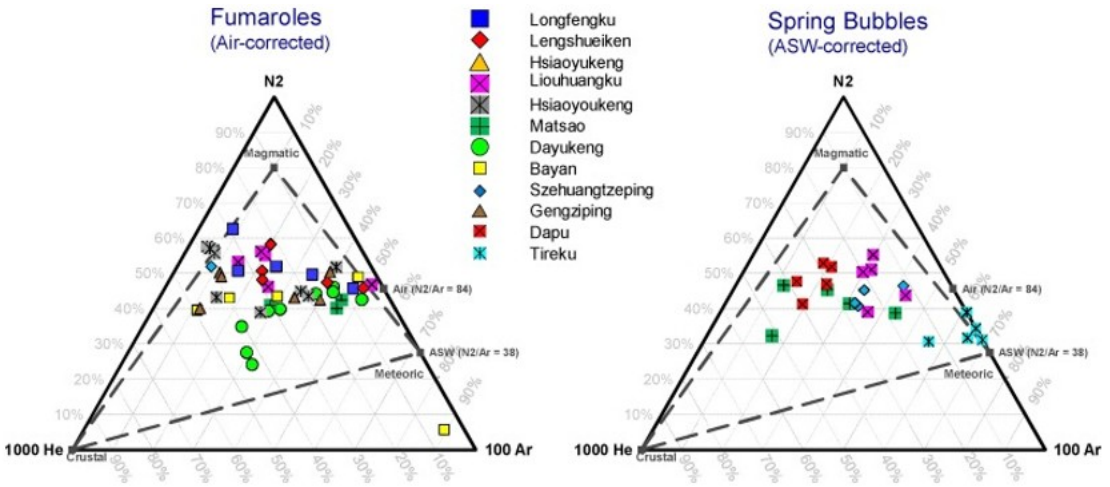

Fig. 15. N_2-He-Ar plots for fumarolic gases (left) and spring gas bubbles (right), using the analyses reported by Lee et al., 2005, Lee et al., 2008, Ohba et al. (2010), and Witt et al. (2008). Such plots have been interpreted by Lee et al. (2008) as evidence for mixing of a meteoric component with convergent plate gases.

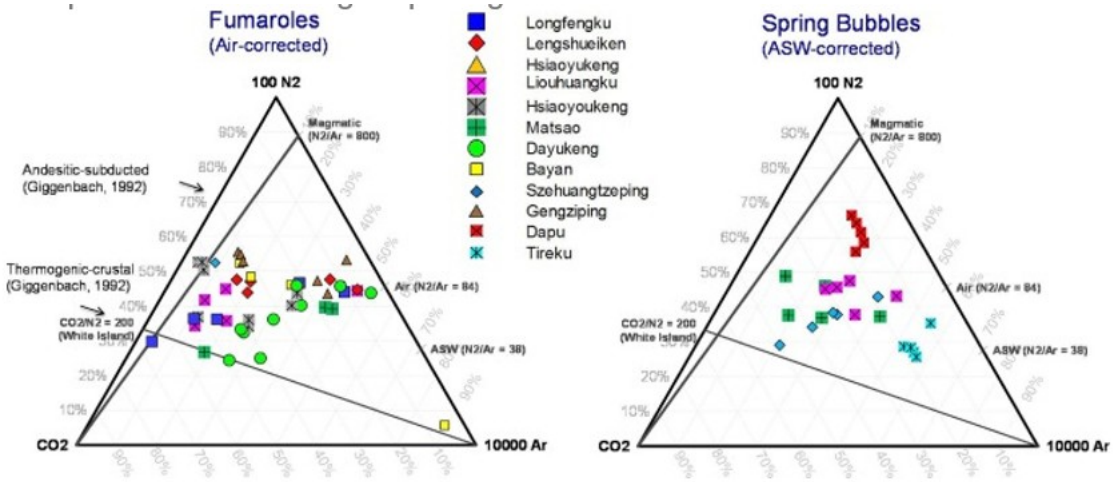

Fig. 16. N_2-Ar-CO_2 plots for fumarolic gases (left) and spring gas bubbles (right), using the analyses reported by Lee et al., 2005, Lee et al., 2008, Ohba et al. (2010), and Witt et al. (2008). The plots show a trend similar to that observed on the N_2-He-Ar plot, revealing a strong meteoric component in many of the samples. The CO_2 content in at Szehuangtzeping (Zone C) appears significantly higher in spring gas bubble samples compared to fumaroles, likely an indication of steam-heated waters.

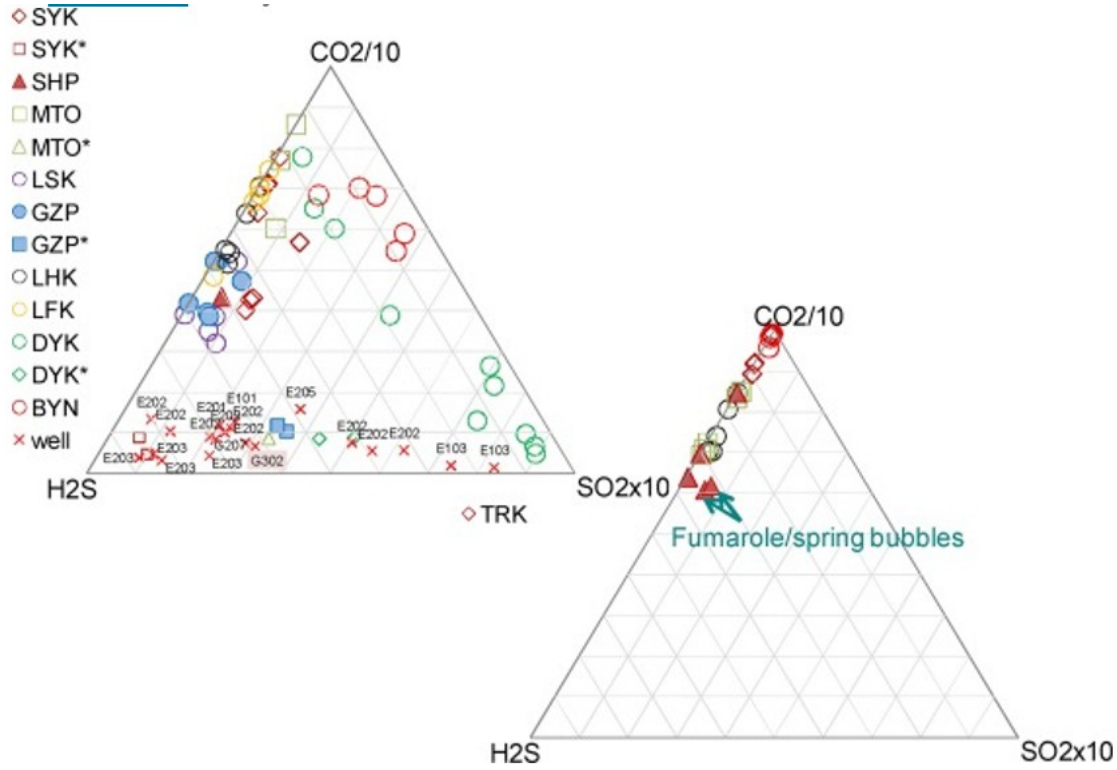

Fig. 17. $CO_2/H_2S/SO_2$ plots of analyses reported for fumaroles(left) and spring gas bubbles (right) by Lee et al., 2005, Lee et al., 2008, Ohba et al. (2010), and Witt et al. (2008). The older data compiled by ITRI (1969–1972) are shown as labeled x symbols (e.g. E202) for wells, and with a location designation in the legend followed by * for fumaroles. The plots show the dominance of SO_2 gas in many of the DYK samples, suggestive of more oxidizing conditions at this location. The plots also reveal a significant composition change between the older (1969–1972) and newer (2003–2007) data. Spring gas bubbles (right) are depleted in SO_2 and H_2S relative to fumaroles (left) because these gases are very soluble in water (thus get scrubbed by water).

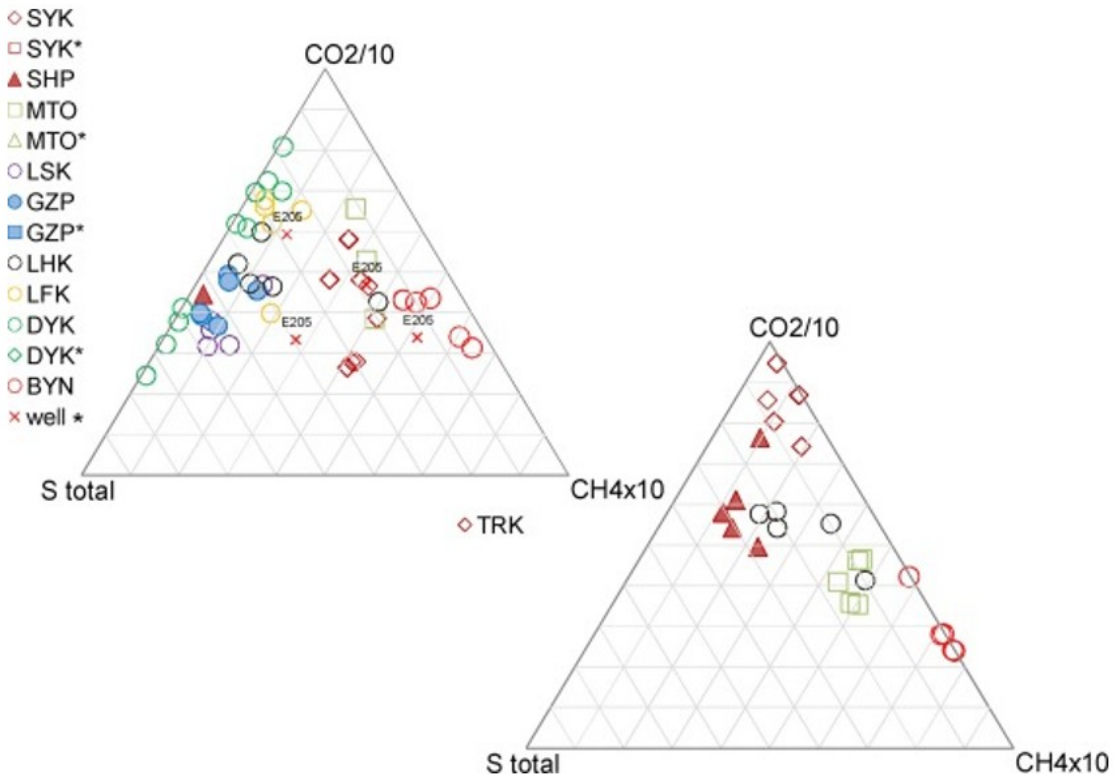

Fig. 18. $CO_2/S_{total}/CH_4$ plots of data reported for fumaroles (left) and spring gas bubbles (right) by Lee et al., 2005, Lee et al., 2008, Ohba et al. (2010), and Witt et al. (2008). S_{total} is $H_2S + SO_2$. A few data points from the ITRI compilation (only data with reported CH_4) are also included, shown as “wells”. Fumaroles from BYN, SYK and MTO appear more reducing than at other locations because of their higher CH_4 content. The concentrations of sulfidic gases in the spring bubbles (right) are lower than in the fumaroles (left), consistent with scrubbing by water.

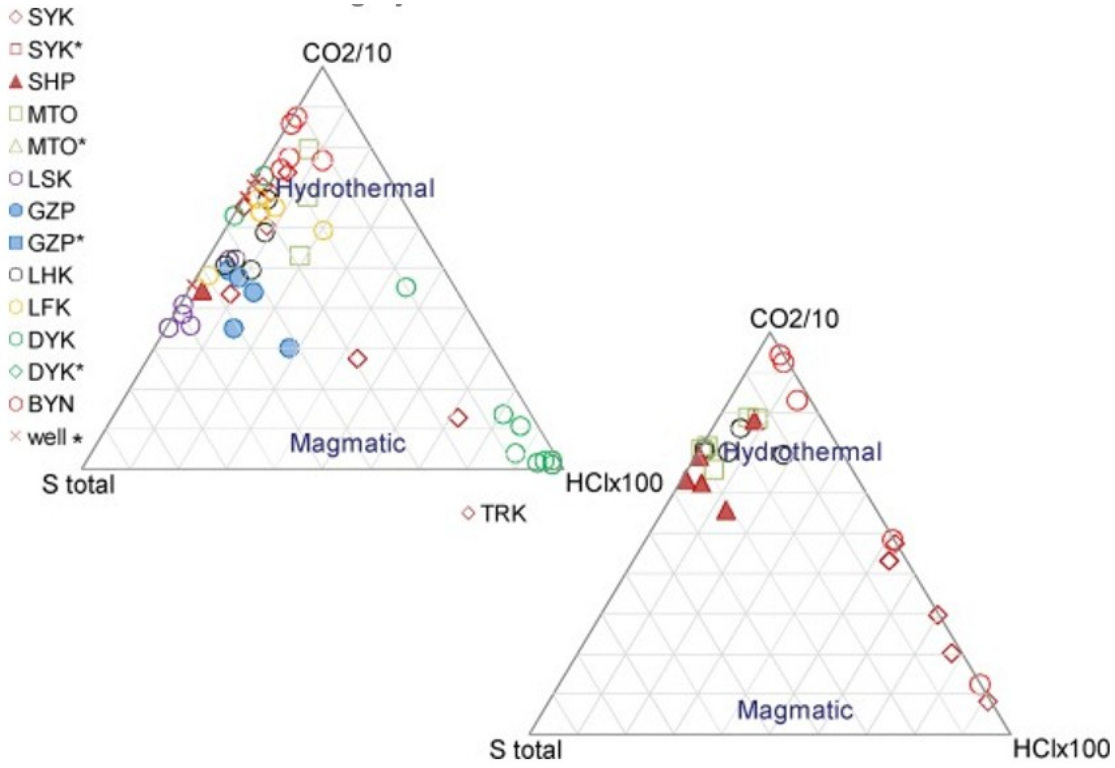

Fig. 19. CO_2/S/HCl plots of data reported for fumaroles (left) and spring gas bubbles (right) by Lee et al., 2005, Lee et al., 2008, Ohba et al. (2010), and Witt et al. (2008). S_{total} is $H_2S + SO_2$. Samples from DYK and some SYK samples stand out with higher HCl concentrations, reflecting a stronger magmatic signature at these locations. Hydrothermal (geothermal) conditions are expected to prevail at $CO_2/S_{total} > 10$ (on the plot, equal amounts of $CO_2/10$ and S_{total}). As noted for other plots, the scrubbing of sulfidic gases in spring waters is likely the reason for the lower concentrations of these gases in the spring gas bubbles (right) compared to the fumaroles (left).

Prior to preparing these gas ternary plots, the gas compositions were corrected for air contamination (for the fumarole samples) and air-saturated groundwater (ASW – for spring gas bubbles). The correction was applied by assuming that all the detected oxygen represents contamination from air or ASW, then removing amounts of Ar, N_2, and He in proportion to the known concentration of these gases in air or ASW.

Our review of the published fumarole and spring gas analyses indicate that the data from the various recent published studies are generally consistent with one another. As a whole, these data clearly show that the composition of fumarolic and spring bubble gases at Tatun represent a mixture of magmatic and meteoric components (Figs. 15and 16), in line with earlier assessments by Lee et al., 2005, Lee et al., 2008 and Ohba et al. (2010). However, the older 1969–1972 data show significantly less CO_2 in the sampled gases than reported in more recent samples (Fig. 17). Whether this difference is real or an artifact of different sampling or analytical procedures is unknown. The plots also show that fumaroles and spring bubbles exhibit a similar range of compositions (except for sulfidic gases, which get scrubbed by water in the spring gases), pointing toward a system chemistry that is likely gas-controlled rather than water-controlled. SO_2 gas is dominant in

many of the DYK samples (Fig. 17), which is indicative of more oxidizing magmatic conditions at this location. This is consistent with the much lower CH_4 concentrations in the DYK samples compared to BYN, SYK and MTO (Fig. 18) where conditions appear more reducing, as previously pointed out by Ohba et al. (2010).

HCl concentrations are higher in most of the DYK and some SYK samples compared to samples collected at other locations (Fig. 19). The presence of elevated HCl in spring-gas bubbles (Fig. 19, right) is questionable, however, because HCl is highly hydrophilic and its vapor pressure in water is low at low temperatures, even at spring pH values near 2. The presence of HCl is typical of magmatic signatures, and Lee et al. (2008) report that DYK gases appear to become more magmatic with time. The ratio of CO_2 to total sulfidic gases (H_2S+SO_2) can also be used to further distinguish magmatic from more hydrothermal (or geothermal) conditions. Ratios greater than 10 can be interpreted as typical of hydrothermal conditions (e.g., Lee et al., 2008). Using this criterion, points in Zone C (SHP and GZP; the area of primary exploration interest), display an intermediate character between truly magmatic and hydrothermal (Fig. 18, Fig. 19).

Because commercial geothermal development of a resource with low pH fluids associated with a volcanic vapor core zone is at least very expensive and commonly impossible, the spatial distribution of H_2S/SO_2 and S_{total}/HCl ratios in fumarole gases was also investigated. This was accomplished by generating contour maps of these ratios (by kriging; Fig. 20, Fig. 21) using the data from Lee et al. (2008) for the time periods 2004, 2005, and 2006. Because there are only a small number of sampled locations, contour plots generated in this manner should be interpreted carefully and contour details between data points should not be given too much weight. Nevertheless, these maps are useful to glance at the general spatial distribution of gas compositions, and may infer the hydrothermal character of areas where data points are available. These maps also show that gas compositions have varied at Tatun from 2004 to 2006. In general, throughout this time period, all three plots indicate that Zone C has maintained higher H_2S/SO_2 ratios (thus a somewhat more hydrothermal character) than adjacent areas further to the SW, which are closer to younger volcanic centers and would be expected to display more magmatic signatures. However, it should be noted that the H_2S/SO_2 ratio at SHP dropped from ~1400 in 2004, to ~900 in 2005 then to 50 in 2006 (the latter low value is difficult to see on Fig. 20 because of the elevated ratio at nearby GZP). The S_{total}/HCl ratio increased at SHP from ~200 to ~700 during this time period (Fig. 21). In contrast to SHP, at GZP, the H_2S/SO_2 ratio increased from ~500 to 2500 between 2005 and 2006 (no 2004 data) and the S/HCl ratio remained at relatively high values of ~500 in 2005 and 800 in 2006. It should be noted that compared to Zone C, more variability and/or lower H_2S/SO_2 ratios are observed in other areas such as BYN and MTO, suggesting that Zone C should be a reasonable first target for geothermal development. It should be noted, however, that the time

period analyzed here is rather short and that conditions at these locations may have changed since 2006.

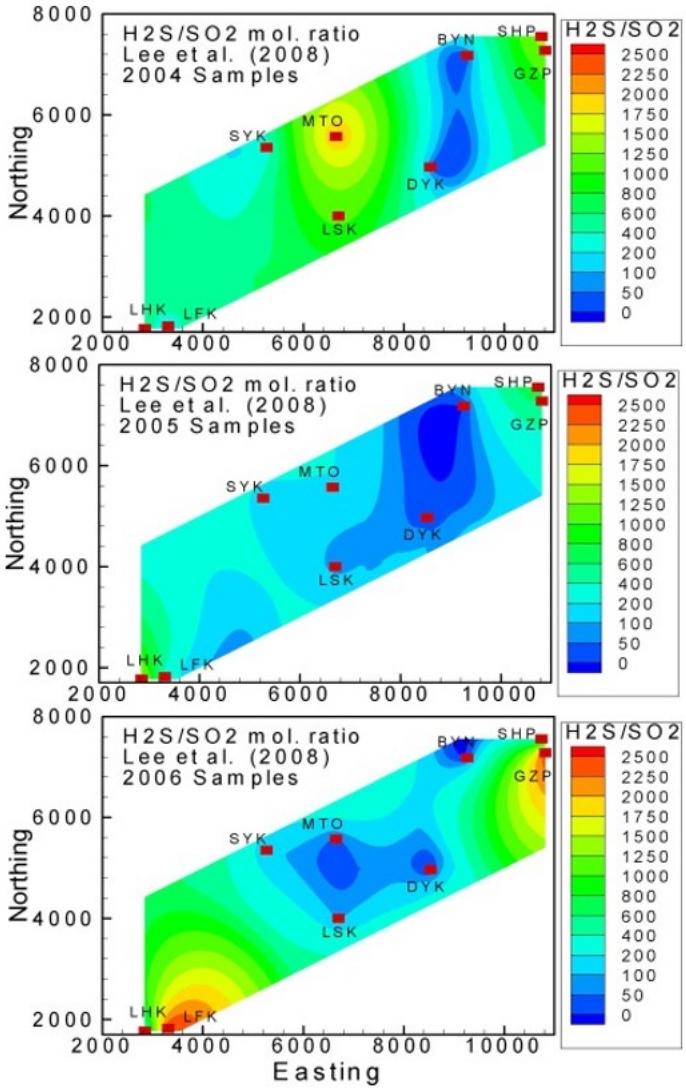

Fig. 20. H_2S/SO_2 contour plots for three time periods (2004, 2005, and 2006) using the data reported by Lee et al. (2008; Lee et al. (2008; note, no data were reported for the GZP point in 2004). Lower ratios indicate higher SO_2 and thus more magmatic/volcanic conditions that are less suitable for geothermal development. Axis coordinates are in UTM (TWD97 datum) – northing values are 278xxxx and easting values are 30xxxx (all values are in m).

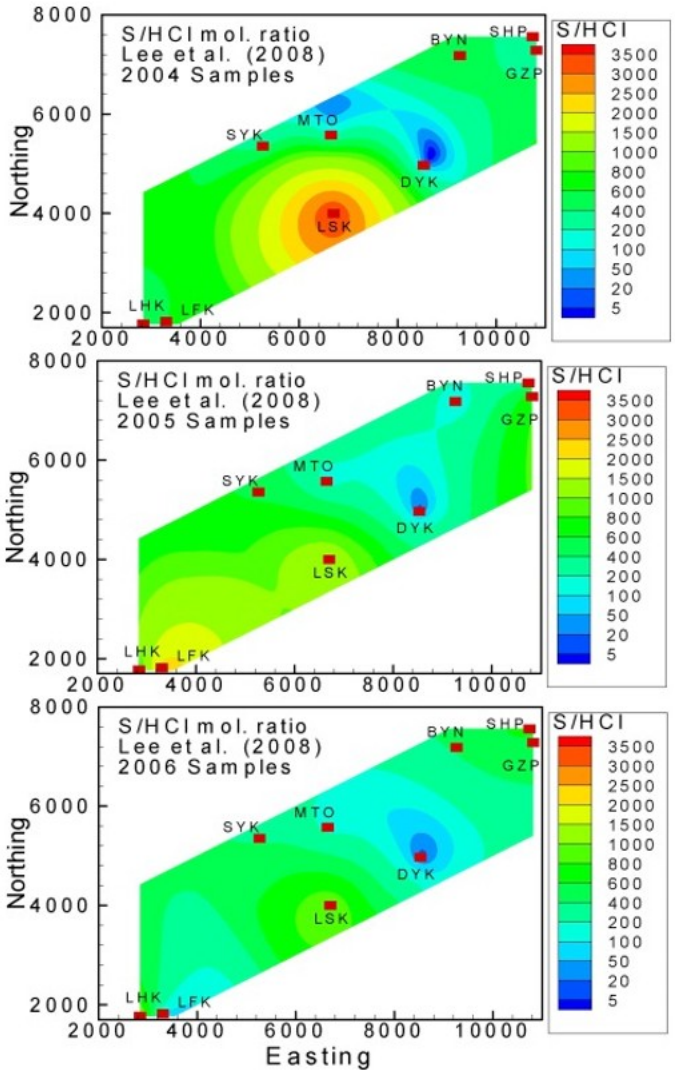

Fig. 21. S_{total}/HCl contour plots (S_{total} is H_2S+SO_2) for three time periods (2004, 2005, and 2006) using the data reported by Lee et al. (2008; Lee et al. (2008; note, no data were reported for the GZP point in 2004). Low ratios indicative of elevated HCl conditions have remained at DYK but varied significantly at LSK. Axis coordinates are in UTM (TWD97 datum) – northing values are 278xxxx and easting values are 30xxxx (all values are in m).

The similarities between the compositions of fumaroles and spring gas bubbles, the spatial variability in gas compositions, and the general absence of mature geothermal waters except possibly at depth as suggested in the Matsao area would suggest a geothermal activity that is most often gas-dominated and likely compartmentalized. Such a conceptualization is illustrated in Fig. 22, which presents an alternative model to that shown in Fig. 11. Such a system has a network of narrow vertical vapor chimneys with localized surrounding liquid-dominated areas. In such a system, the strong acidic alteration results from the reaction of upflowing magmatic hydrothermal vapors with rocks and downward-flowing steam-heated waters from the near surface, with more neutralization expected in the andesitic rocks than in the underlying feldspar-poor sandstones (Liu et al., 2011).

Alteration is expected to result primarily from H_2SO_4, at least away from Dayukeng (DYK) where the highest HCl concentrations are detected in fumaroles. In such a system, deep zones in andesitic rocks away from the chimneys would be expected to exhibit propylitic alteration, as found in the deep portions of Matsao well E-205, indicative of liquid-dominated conditions (Giggenbach, 1997). The Biliran (Ramos-Candelaria et al., 1995; Apuada et al., 2010) and Alto Peak (Reyes et al., 1993) systems in the Philippines could be viewed as analogues to such a system. The extent of such liquid-dominated areas at Tatun are unknown, but their occurrence would be more likely in areas exhibiting higher CO_2/S_{total}, H_2S/SO_2 and S_{total}/HCl ratios compared to other areas. Zone C seems to correspond to such an area. It should be noted that the area comprising LHK and LFK to the southwest share some of the same characteristics but were not considered further because they are located closer to urban development and are near low pH outflow springs.

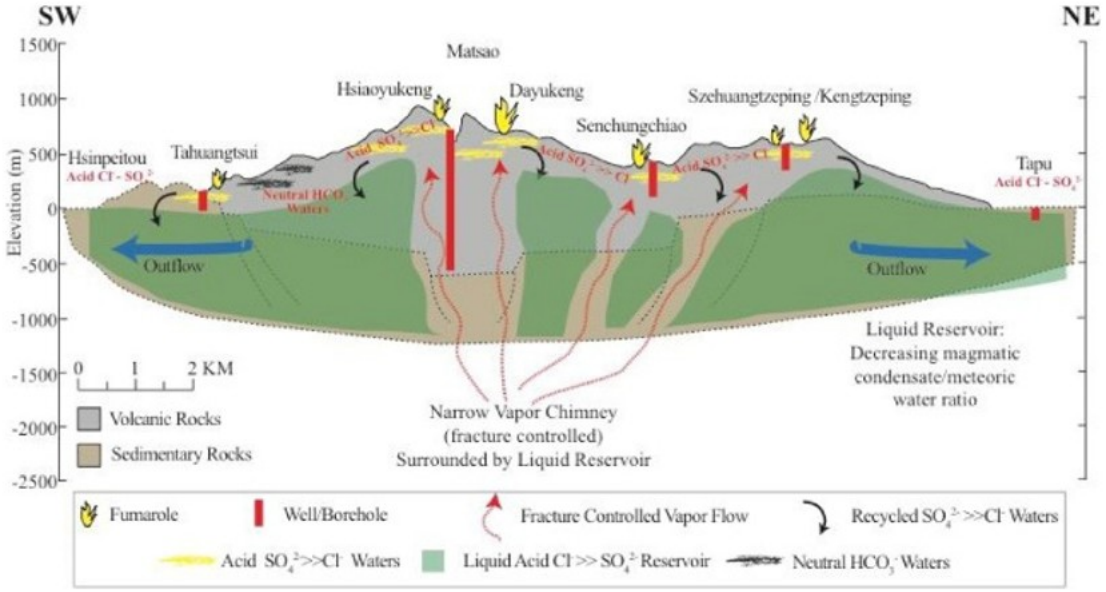

Fig. 22. Updated geochemical conceptual process sketch of a hybrid vapor- and liquid-dominated system consistent with the propylitic alteration observed in deep Matsao wells, and the gas composition variability observed at Tatun.

3.5. Geothermometry

Our review of spring and well water chemistries showed that except possibly for deep water initially sampled in Matsao well E-205, the thermal waters at Tatun are immature, meaning that they do not represent reservoir fluids that have reached some degree of chemical equilibrium with reservoir rocks. These spring and well waters represent mostly meteoric groundwater that has interacted with volcanic gases, and therefore are not suitable for solute geothermometry analyses.

For this study, gas geothermometers were selected on the basis of: (1) the type of gas species analyzed most often (e.g., H_2S, SO_2, CO_2, CH_4) and (2) the

geothermometers found to yield temperatures most consistent with measured temperatures in areas where both gas composition and deep temperatures have been measured, such as in deep Matsao wells. Our first choice focused on geothermometers based on SO_2/H_2S ratios (Giggenbach, 1987) and on CO_2/CH_4 ratios Giggenbach (1997), because of the large amount of concentration data available for these gases. Both these geothermometers, however, require an estimate of reservoir redox conditions.

Following the approach of Giggenbach (1981), redox conditions can be characterized by the R_H variable, which represents the ratio of the hydrogen to water fugacities in the system (i.e., $R_H = f_{H2}/f_{H2O}$). The use of the R_H variable presents an advantage over using other redox variables (such as oxygen fugacity) because it relies on physical quantities of H_2 and H_2O. Also, R_H remains essentially constant as a function of temperature in systems where redox equilibrium is buffered by Fe(II)/Fe(III) in rocks (i.e., FeO/Fe_2O_3), at a value of about −2.8.

Giggenbach (1981) suggested that an R_H value of −2.8 should be appropriate for most hydrothermal systems. However, at Tatun, the presence of SO_2 in fumaroles suggests more oxidizing conditions than the Fe(II)/Fe(III) rock buffer. In fact, at temperatures below ~400 °C, gas equilibrium plots presented by Giggenbach (1987) for the study of volcanic White Island show that the stability fields of CH_4/CO_2 and H_2S/SO_2 as a function of R_H do not overlap. Our own calculations for the equilibrium reaction $3CH_{4(g)} + 4SO_{2(g)} = 3CO_{2(g)} + 4H_2S_{(g)} + 2H_2O_{(g)}$ also show that measurable concentrations of CH_4 and CO_2 cannot be at thermodynamic equilibrium with measurable H_2S and SO_2 at low temperatures. The fact that these four gases are typically present in measurable quantities in Tatun gases implies that the CH_4/CO_2 and H_2S/SO_2 redox couple are at disequilibrium, and therefore that the same R_H cannot be used for the CH_4/CO_2 and the H_2S/SO_2 geothermometers. For this reason, for each of these geothermometers, the $R_H$was “calibrated” by comparing measured and calculated temperatures in deep Matsao wells, the only location for which deep measured downhole temperatures and corresponding gas compositions were found. As shown in Table 1, reasonable results were obtained using $R_H \sim -5$ for the SO_2/H_2S geothermometer, and $R_H \sim -3$ for the CO_2/CH_4 geothermometer. These values were thus used for subsequent geothermometry analyses at locations other than Matsao. As shown on Table 1, temperatures calculated with these geothermometers increase with increasing R_H(less negative values, more reducing conditions). Therefore, because Zone C may exhibit R_H values more reducing (less magmatic) than at Matsao, predicted temperatures in Zone C using R_H values calibrated for Matsao should be regarded as minimum values. It should also be noted that any gas geothermometry results should be interpreted with a large uncertainty envelope, likely at least ±20 °C in the present case given the

small number of data points for which measured and calculated temperatures can be compared.

Table 1. Application of the SO_2/H_2S and CO_2/CH_4 gas geothermometers with data from deep Matsao wells, using different R_H values, and comparisons with measured downhole temperatures.

Location	SO_2/H_2S T(°C)		Measured
	$RH = -3$	$RH = -5$	T(°C)
Well E203	460	247	241
Well E203	466	250	241
Well E203	471	252	241
Well E203	486	260	241
Well E201	486	260	236

Location	CO_2/CH_4 T(°C)		Measured
	$RH = -3$	$RH = -5$	T(°C)
Well E205	234	−3	232
Well E205	237	−2	232
Well E205	269	7	232
Well E205	220	−7	232

Other gas geothermometers were also tested. In all, the following geothermometers were applied to available gas analyses for both fumaroles and spring gas bubbles:

H_2S/SO_2 at $R_H = -5$ (Giggenbach, 1987)

CH_4/CO_2 at $R_H = -3$ (Giggenbach, 1997)

H_2/Ar at $R_H = -5$ (Giggenbach, 1991)

CO_2/Ar (Giggenbach, 1991)

In addition, geothermometer cross-plots using the Excel spreadsheet developed by Powell and Cumming (2010)were constructed, including:

H_2/Ar versus CO_2/Ar (Giggenbach, 1991)

CO/CO_2 versus CH_4/CO_2 at $R_H = -3$ (Giggenbach, 1991)

Results of individual geothermometers are shown in Table 2for Zone C. Preference is given to the SO_2/H_2S and CO_2/CH_4 results because these were tested and/or calibrated against available temperatures at Matsao (Table 1). Unfortunately, the concentration of Ar was not measured in the gases at Matsao. In addition, at locations where Ar data are available, an effect of the strong meteoric component on Ar-based geothermometry cannot be ruled out, even though the gas analyses were corrected for contamination by air (fumaroles) and air-saturated groundwater (spring bubbles). The results in Table 2suggest that reservoir temperatures between about 200 and 300 °C could possibly prevail in Zone C, keeping in mind the high uncertainty of such analyses. The cross-plot geothermometers in Fig. 23, Fig. 24 for H_2/Ar vs. CO_2/Ar and CH_4/CO_2 vs. CO/CO_2 also suggest temperatures in this range for Zone C. One important caveat is that the Zone C area is on the margins of the Tatun system, and that the calculated equilibrated temperature values could represent conditions more indicative of the main reservoir to the southwest. These figures and the other temperature data in Table 2 indicate a reasonable agreement between the ranges of temperatures computed from fumaroles and spring bubble gases.

Table 2. Application of the SO_2/H_2S and CO_2/CH_4 gas geothermometers with gas analyses collected in Zone C (GZP and SHP).

Calculated Temperatures (°C)							
	H_2/Ar		**CO_2/Ar**	**SO_2/H_2S**		**CO_2/CH_4**	
Location	**RH = −3**	**RH = −5**	**Not RH-Dependent**	**RH = −3**	**RH = -5**	**RH = −3**	**RH = −5**
GZP Fumarole	184	327	266	424	**229**	260	4
GZP Fumarole	140	282	263	396	**214**	288	12
GZP Fumarole	139	281	302	457	**246**	283	10
GZP Fumarole	104	247	300	473	**254**	282	10
GZP Fumarole	166	309	242	461	**247**	264	5
SHP Fumarole	205	348	314	463	**249**	305	16
GZP Fumarole	148	291	298			288	12

Calculated Temperatures (°C)

	H_2/Ar		CO_2/Ar	SO_2/H_2S		CO_2/CH_4	
Location	**RH = −3**	**RH = −5**	**Not RH-Dependent**	**RH = −3**	**RH = -5**	**RH = −3**	**RH = −5**
SHP Well G302				497	**265**		
GTP Fumarole				503	**268**		
GTP Fumarole				501	**267**		
SHP Spring Bubble	125	268	291	377	**204**	270	7
SHP Spring Bubble	125	268	285	470	**252**	262	5
SHP Fumarole/Spring Bubble	167	310	301	407	**220**	283	10
SHP Fumarole/Spring	163	306	284	416	**224**	249	1

Calculated Temperatures (°C)							
	H_2/Ar		CO_2/Ar	SO_2/H_2S		CO_2/CH_4	
Location	**RH = −3**	**RH = −5**	**Not RH-Dependent**	**RH = −3**	**RH = -5**	**RH = −3**	**RH = −5**
Bubble							
SHP Fumarole/Spring Bubble	68	211	268	474	**254**	272	7

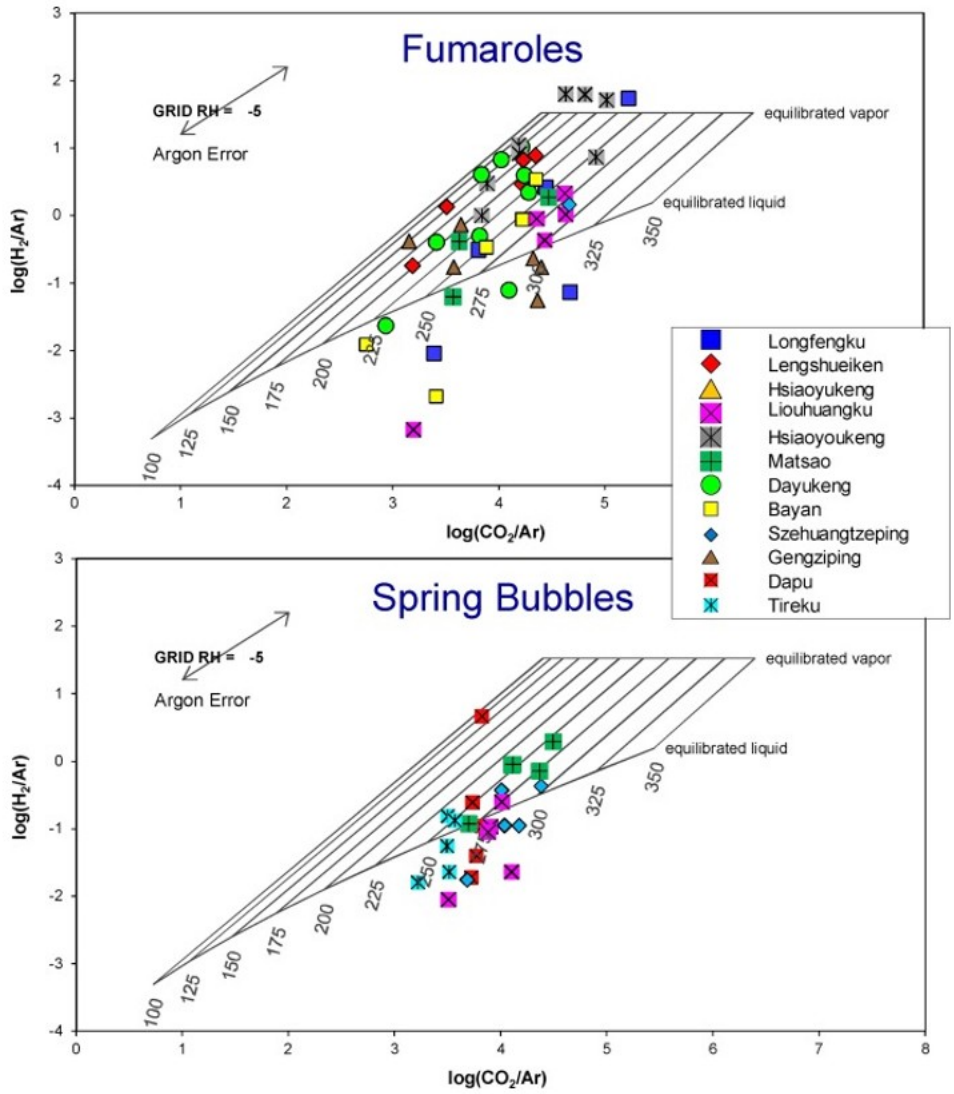

Fig. 23. Cross-plots of the H_2/Ar and CO_2/Ar gas geothermometers using gas analyses reported for fumaroles(top) and spring gas bubbles (bottom) by Lee et al., 2005, Lee et al., 2008, Ohba et al. (2010), and Witt et al. (2008).

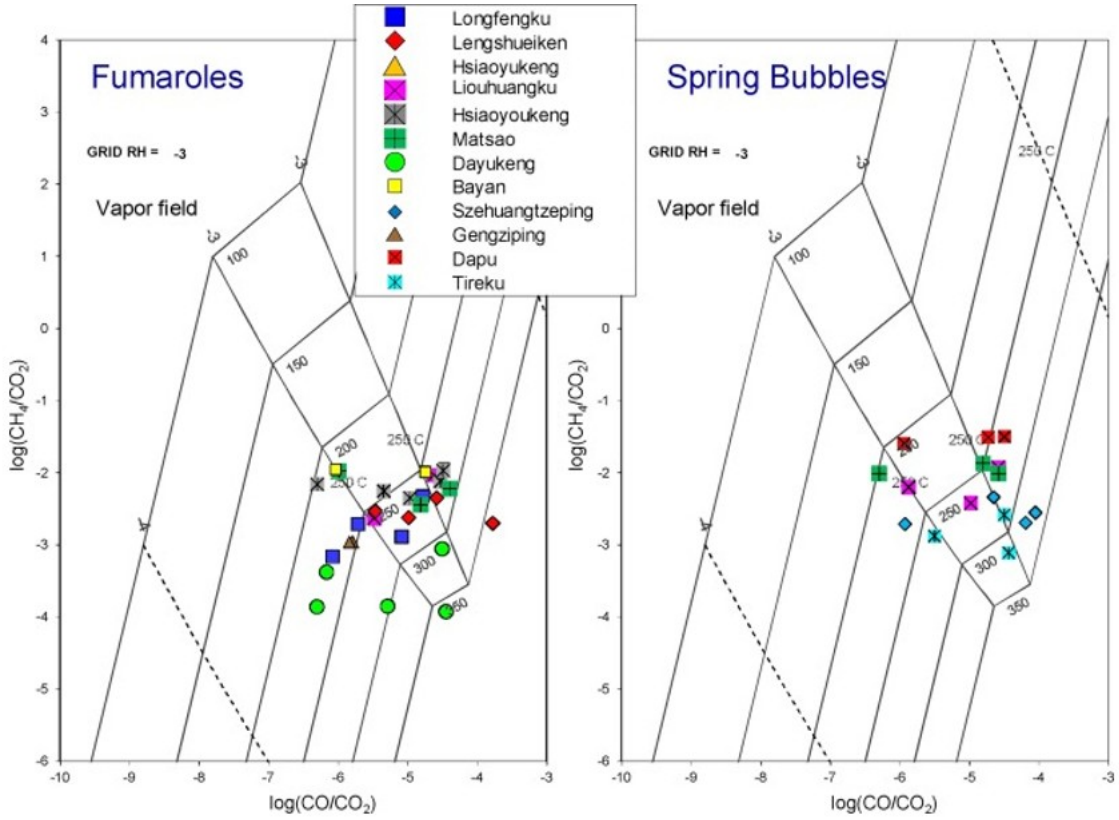

Fig. 24. Cross-plots of the CH_4/CO_2 and CO/CO_2 gas geothermometers using gas analyses reported for fumaroles(left) and spring gas bubbles (right) by Lee et al., 2005, Lee et al., 2008, Ohba et al. (2010), and Witt et al. (2008).

The SO_2/H_2S gas geothermometer may be the most useful geothermometer in this study because a large number of analyses are available for these gases at Tatun, and this geothermometer has been shown to work reasonably well with fumaroles in previous studies (Giggenbach, 1987). This geothermometer yields temperatures in the 220–270 °C range in Zone C (results highlighted in bold in Table 2), which is also mostly consistent with results of the H_2/Ar-CO_2/Ar and CO_2/CH_4-CO/CO_2 geothermometers, which yield a broader temperature range of ~200–300 °C. A general trend from hotter subsurface temperatures around DYK to cooler temperatures away from this area is predicted, which is in line with our current knowledge of the Tatun volcanic zone.

4. Resistivity analysis of Tatun

Resistivity surveys are commonly conducted during geothermal exploration to help map the extent of the clay cap associated with the geothermal system (e.g., Ussher et al., 2000). Magnetotelluric (MT) data were acquired in the study area between 2008 and 2015. Fig. 25 shows the locations of MT stations acquired over the area of interest, topography, power line locations, the National Park boundary, and the Zone C outline. Fig. 25a shows the entire area, while Fig. 25b expands Zone C. The resistivity model from 3D inversion of MT data collected between 2008 and 2014 indicated that the

clay cap extended from the central upflow area up to the NE; however, there were indications that the clay alteration became more discontinuous near Zone C (Fig. 26). To address the need for improved resolution near the area of interest, data were collected at additional MT stations for Zone C in 2015. Most of the older data were collected in a single station mode, some had a remote reference, while the 10 recordings in Zone C acquired in 2015 all used a multi-station mode with a quiet (i.e., high quality) remote reference. Data from 60 MT stations were available for 3-D inversion. A dense grid of power lines posed a challenge to data processing, and some stations and some frequencies had to be excluded from the inversion because of a high level of cultural noise (e.g., A24, D13, D19, D86, YM-9, YM-10, YM-28, YM-31, N03, and N08). With the exception of stations N03 and N08, all excluded stations were on the periphery of the study area.

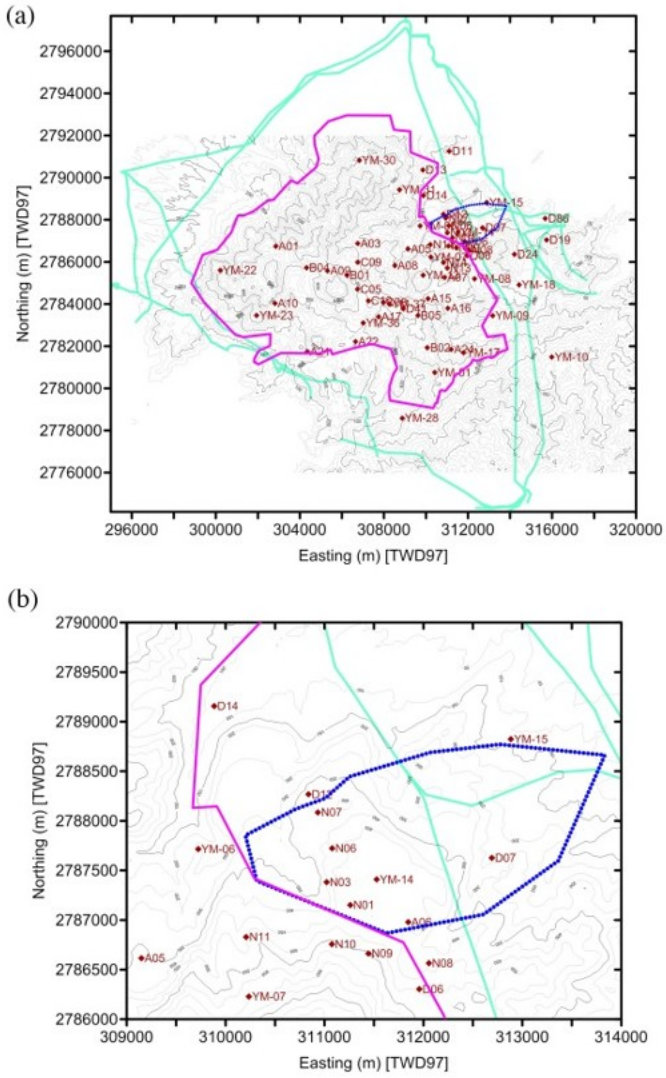

Fig. 25. (a) Topo map of entire study area, (b) zoom on Zone C. Power lines are shown by light green color, the outline of Zone C is shown in dark blue, the National Park boundary is shown in magenta, and MT stations locations are shown by red labeled symbols.

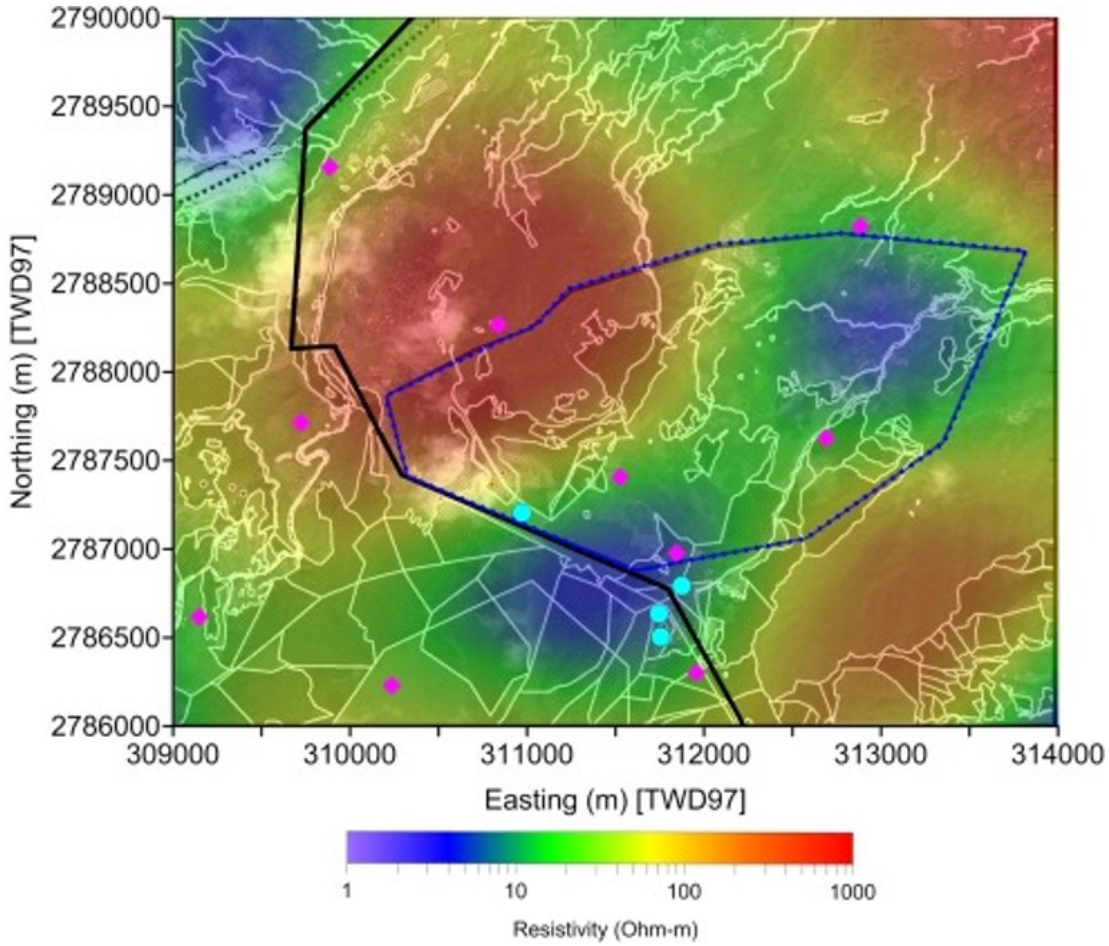

Fig. 26. Resistivity map from 3-D MT model using 2008–2014 MT data at the depth of 500 m (from the ground surface) in Zone C (depicted by dark blue line) and its vicinity. MT station locations are shown by magenta diamonds, geochemical sampling locations are shown by cyan circles, and the National Park boundary is shown by thick black line.

Two 3-D inversion codes were used to invert 3-D MT data for Tatun. ITRI researchers used a data domain inversion algorithm WSINV3DMT (Siripunvaraporn, 2011; Siripunvaraporn and Egbert, 2009; Siripunvaraporn et al., 2005), which uses a data-space variant of the minimum-structure Occam inversion approach. LBNL researchers used a model space inversion algorithm EMGeo (Newman and Alumbaugh, 2000; Newman et al., 2003), which uses a nonlinear conjugate-gradient optimization scheme with an approximate Hessian as a pre-conditioner (Newman and Boggs, 2004); in this inversion method, the topography is built into the model. The inversion parameters (starting model, treatment of regional water bodies, model grid spacing, iteration procedure, regularization, termination) are in keeping with the methods implemented by previous studies (e.g., Gasperikova et al., 2015, Lindsey and Newman, 2015). A NE-SW resistivity profile through the area of interest from the ITRI inversion is depicted in Fig. 27. The final 3-D resistivity model recovered by EMGeo is shown in Fig. 28. Resistivity values of 15–17 ohm m (light blue color) are used to outline a possible clay cap/seal.

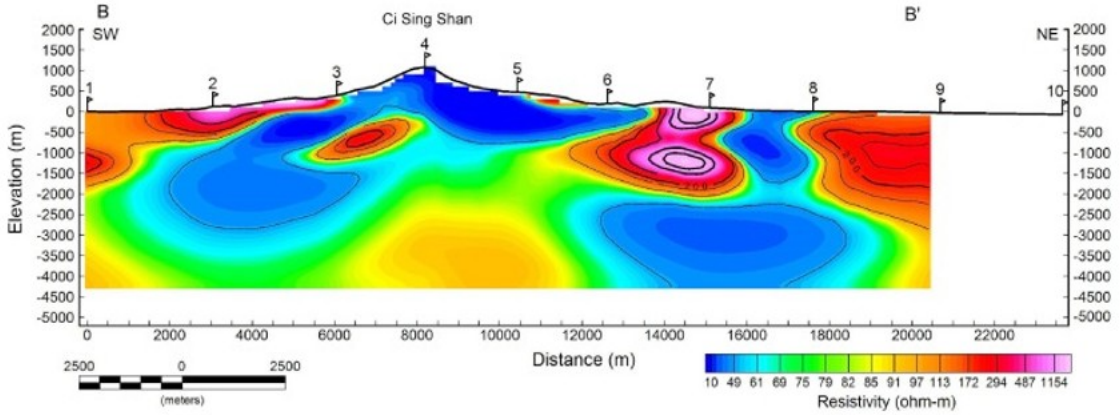

Fig. 27. Resistivity cross-section along profile B (equivalent to B-B’ in Fig. 1) as recovered by 3D MT inversion. The site of interest in Zone C is projected near flag 6 (flags represent projected MT station locations along the profile).

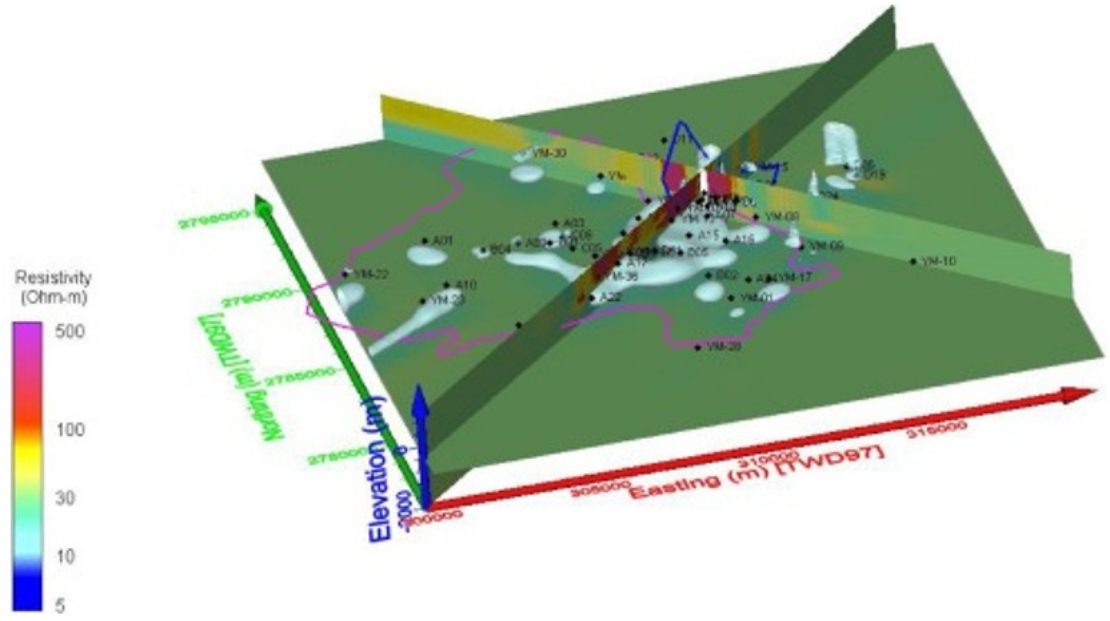

Fig. 28. Resistivity model of the TVG as obtained by 3-D MT inversion using EMGeo with 15–17 ohm m isosurface. The ITRI exploration well (see plotted location in Fig. 1, Fig. 31) is shown as a white vertical line where two 2D sections intersect, the outline of Zone C is shown in dark blue, and the National Park boundary is shown in magenta.

Fig. 29 shows the elevation of the 10–17 ohm-m zones for the zoomed view in the vicinity of Zone C. 10–17 ohm-m resistivities for the entire Tatun area were found at elevations ranging between −500 to 900 m above sea level (masl): this wide range in the base of the clay cap elevations reflects the significant topography of the region, with higher elevation clay cap values found in the higher elevation regions. A similar low resistivity feature, also interpreted to represent a clay cap, was identified beneath Chishinshan and the Matsao and Da-you-keng (DYK) thermal areas in an audio-magnetotelluric (AMT) survey of the central Tatun region (Komori et al., 2014) – the AMT study did not extend over to the area of Zone C. For the ITRI

well location, the base of the clay cap is estimated to be located at an elevation between −100 to 0 masl.

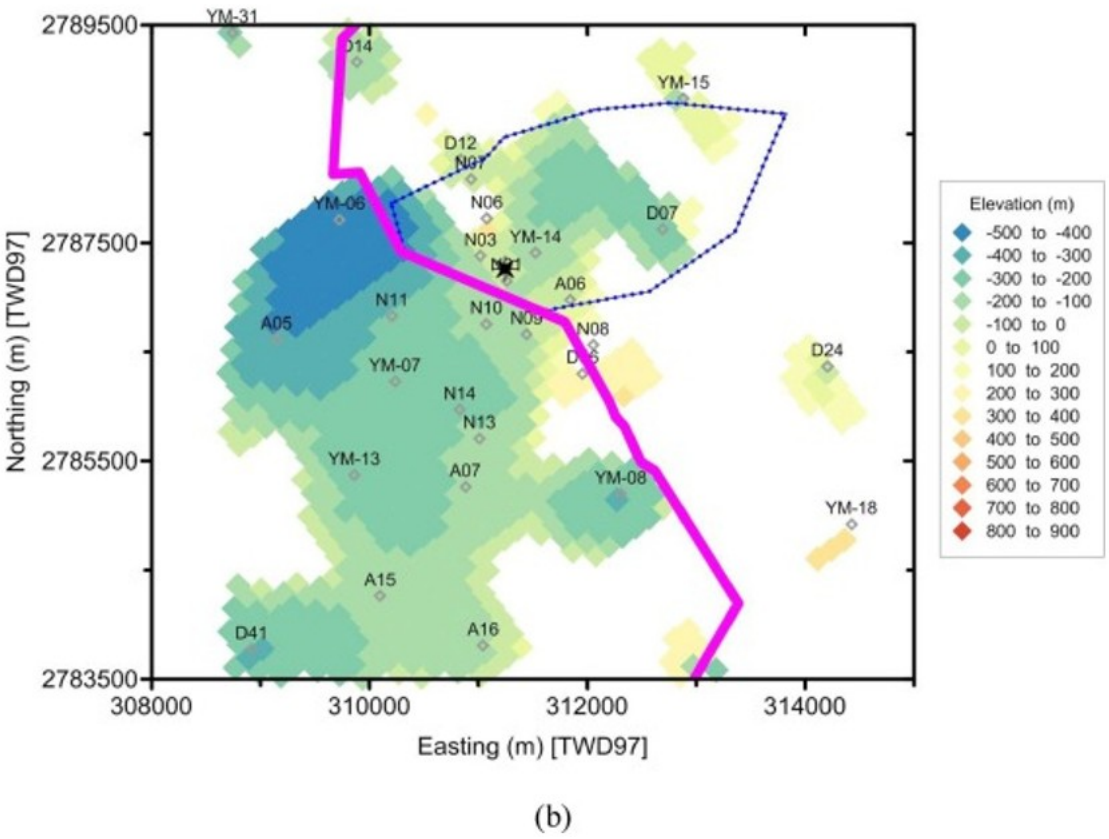

(b)

Fig. 29. Elevation of the bottom of the clay-rich seal (defined by resistivity values of 10–17 ohm m) for the area in the vicinity of Zone C. The outline of Zone C is shown in dark blue, the National Park boundary is shown in magenta, MT stations are shown by grey symbols, and the black star indicates the ITRI well location.

A limited model appraisal was done with sensitivity studies based upon different starting models (WSINV3DMT), and by modifying model structure and evaluating the impact on the model data fit (EMGeo). To validate or verify if the seal structure from Zone C to the main Matsao area is continuous we added a low resistivity structure. While the changes to the model were very small, the data fit at the closest stations to that area worsened, suggesting that the recovered structure in our model is a better fit and that the seal structure is heterogeneous as suggested by our model.

Acquiring new high-quality MT data significantly improved the model in Zone C. The models suggest that the clay cap/seal present in the TVG is heterogeneous in nature but extends to Zone C and the location of the ITRI exploration well. This site appears to be near the outer margin of the high temperature geothermal system, as suggested by the lower temperatures (~160 °C) encountered by the nearby CPC-SHP-1T well, as discussed in Section 5.

5. Conceptual model for Tatun

5.1. General conceptual model for Tatun

Conceptual models serve as a methodology for integrating diverse data sets into a coherent representation of the key elements of geothermal systems (e.g., Cumming, 2016). Conceptual models can be used to locate drilling targets and identify data gaps and uncertainties. These models are updated as new ideas and data are developed.

Conceptual models highlight the following key components of geothermal systems:

• Heat source (temperature distribution).

• Fluid flow (permeability distribution).

• Reservoir seal (clay cap).

• Volume (resource boundaries).

• Recharge and fluid chemistry (sustainability, fluid chemistry, and water-rock interaction).

These components reflect the major processes (such as heat and fluid flow and water-rock interaction) that control the development of hydrothermal systems.

An early conceptual model of the Tatun system was presented by Chen (1975). Chen's model depicted the principal upflow zone in the Matsao area, and interpreted the acid nature of the geothermal fluids to indicate a large volcanic component in the geothermal fluids. Fig. 30 depicts our updated version of this model, which incorporates all of the new data available for Tatun. The heat source for the geothermal system is interpreted to be magma chambersand cooling young intrusive rocks associated with the Tatun Volcano Group. The most recent volcanic activity is associated with the Chihsingshan Volcano subgroup (Tsai et al., 2010). These young volcanic rocks also host the most active and oxidized geothermal features, namely the Hsiaoyukeng, Matsao, and Dayukeng fumaroles and associated acid hot springs.

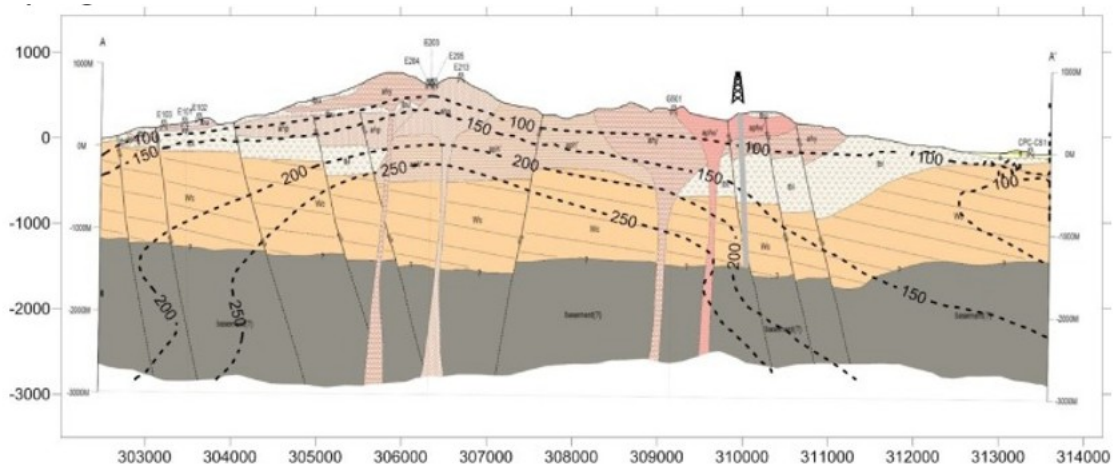

Fig. 30. Conceptual model cross section through the Tatun geothermal system with the location of the new ITRI well. Isotherms incorporate the results of the CPC-SHP-1T well (whose location projects just east of the large well symbol), and indicate that the Zone C location (indicated by a well symbol) is on the margins of the Tatun geothermal system. See Fig. 1 for map legend and location of cross section (A-A').

The main structural fabric of this area consists of NE-SW striking faults, which appear to define the extent of the geothermal system between the Shanchiao normal fault(also known as the Chinshan fault) and the Chilian lineament. The Tatun region is in a very tectonically active region − it is interpreted to have undergone a transition from a zone of compression to one of crustal extension (Wang et al., 1999). Two main outflow zones have been identified: one to the SW of the upflow zone, in the region of Hsinpeitou, and another outflow plume to the NE, associated with the Jiatou and Tapu thermal features.

Resistivity models developed from magnetotelluric surveys of the Tatun area (described in Section 4) indicate the presence of a conductive cap overlying the high temperature reservoir – this zone is inferred to represent clay (argillic) alteration as has been confirmed by petrographic studies of core and cuttings from deep wells in the central portion of the system (e.g., Lan et al., 1980; Chen and Yang, 1984). The extent of the system may be indicated by the spatial distribution of the cap, whose margins coincide with Zone C, where it transitions into a thinner, more heterogeneous feature. This transition occurs near the CPC-SHP-1T well, which lies outside of the high temperature (>200 °C) reservoir.

One key aspect of the Tatun geothermal system is the presence of corrosive, acidic fluids, indicative of a significant volcanic contribution to the system, either from input from magmatic fluids or through interaction with sulfur-rich volcanic rocks (e.g., Ellis and Giggenbach, 1971; Ohsawa et al., 2013). Elevated $^{3}He/^{4}He$ ratios (4.0–7.6 Rc/Ra) measured in fumarole gas samples from Tatun also support a significant magmatic gas component (Yang et al., 1999; Lee et al., 2008). Thus, for this system to be commercially viable, it is critical that neutralization of these fluids through water-rock interaction occurs. The presence of calcite in some deep core samples from Tatun suggests that there are portions of the system that do have more benign fluids. However, past exploration efforts were thwarted by the repeated presence of low pH fluids that dissolved casing. The quartz-rich Wushishan sandstoneunderlying the Tatun volcanic sequence may not be very effective in neutralizing acidic fluids. Use of analog examples from similar systems in the Philippines and elsewhere (e.g., Ramos-Candelaria et al., 1995; Apuada et al., 2010; Tamboboy et al., 2015) may serve as a guide for how such a system could be successfully explored and developed.

5.2. Conceptual model for zone C

The key challenge for exploration at Tatun is to encounter sufficient temperature, permeability, and non-corrosive fluids on the margins of the central upflow zone. Given the presence of Yangmingshan National Park, the

current exploration strategy is to look for geothermal resourcesoutside of the park. Geologic, geophysical, and geochemical data presented in earlier sections suggest that the NE margins of the Tatun system near the She-huang-ping (SHP) and Genziping (GZP) thermal areas (Zone C – Fig. 31) may have commercial reservoir temperatures (≥200 °C) and permeability and non-corrosive fluids (Fig. 30). This was the basis for targeting the ITRI exploration well in Zone C between the two sets of fumaroles.

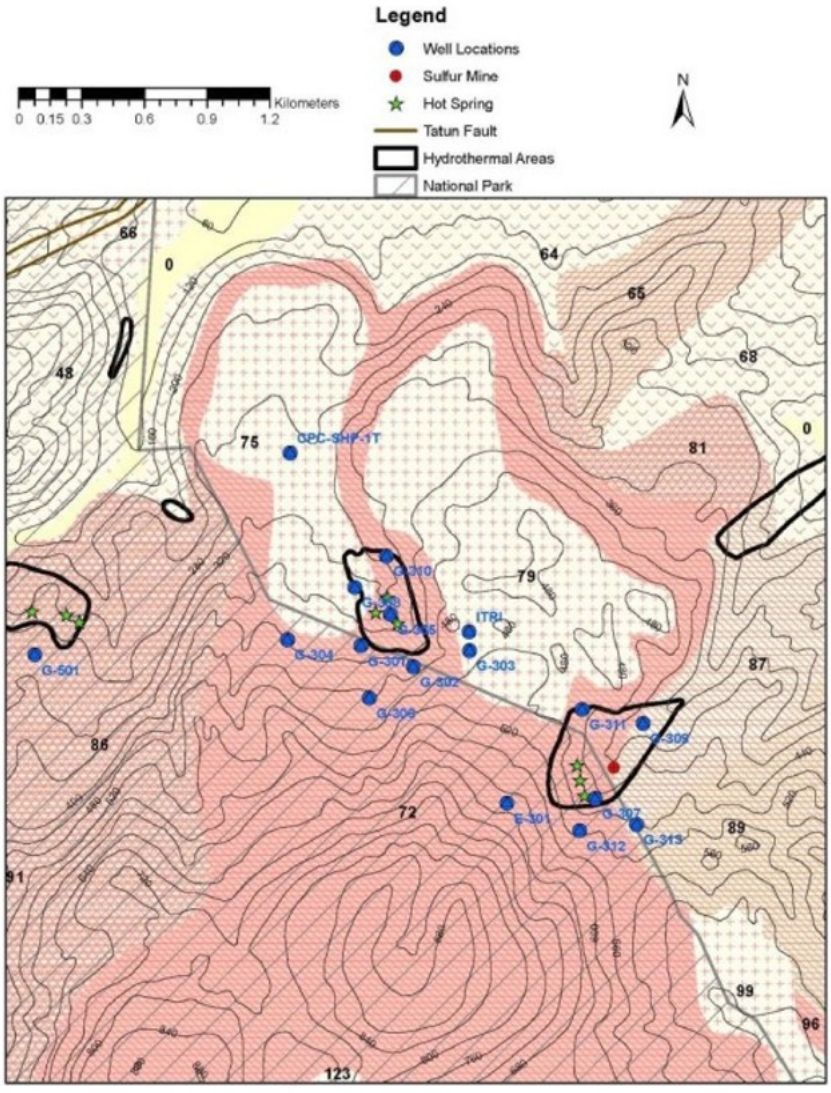

Fig. 31. Geologic map of Zone C with locations of thermal features (stars), temperature gradient wells (blue dots), and hydrothermal alteration areas (black outlines). The location for the new ITRI exploration well (labeled ITRI) is adjacent to the G-303 gradient well.

A conceptual model of the Tatun geothermal system (Fig. 30) indicates an upflow area in the central volcanic portion of the system, with lateral outflow to the NE towards Zone C. The observed thermal gradients in the G-501, E-301, and CPC-SHP-1T wells (Fig. 32) suggest that more modest temperatures will be encountered in the new ITRI exploration well (~150 °C at 1200 m

depth) than those estimated from gas geothemometry. The CPC-SHP-1T well, located ~1.2 km further away (Fig. 31) and drilled to a depth of 2 km, only encountered temperatures slightly above 160 °C. This suggests that the SHP region is on the outer margin of the Tatun hydrothermal system, consistent with the MT results described previously. The discrepancy between these lower predicted temperatures for the ITRI well and the higher gas geothermometry estimates from the SHP and GZP fumaroles may result from the gases having equilibrated from the higher temperature portion of the geothermal reservoir located to the SW.

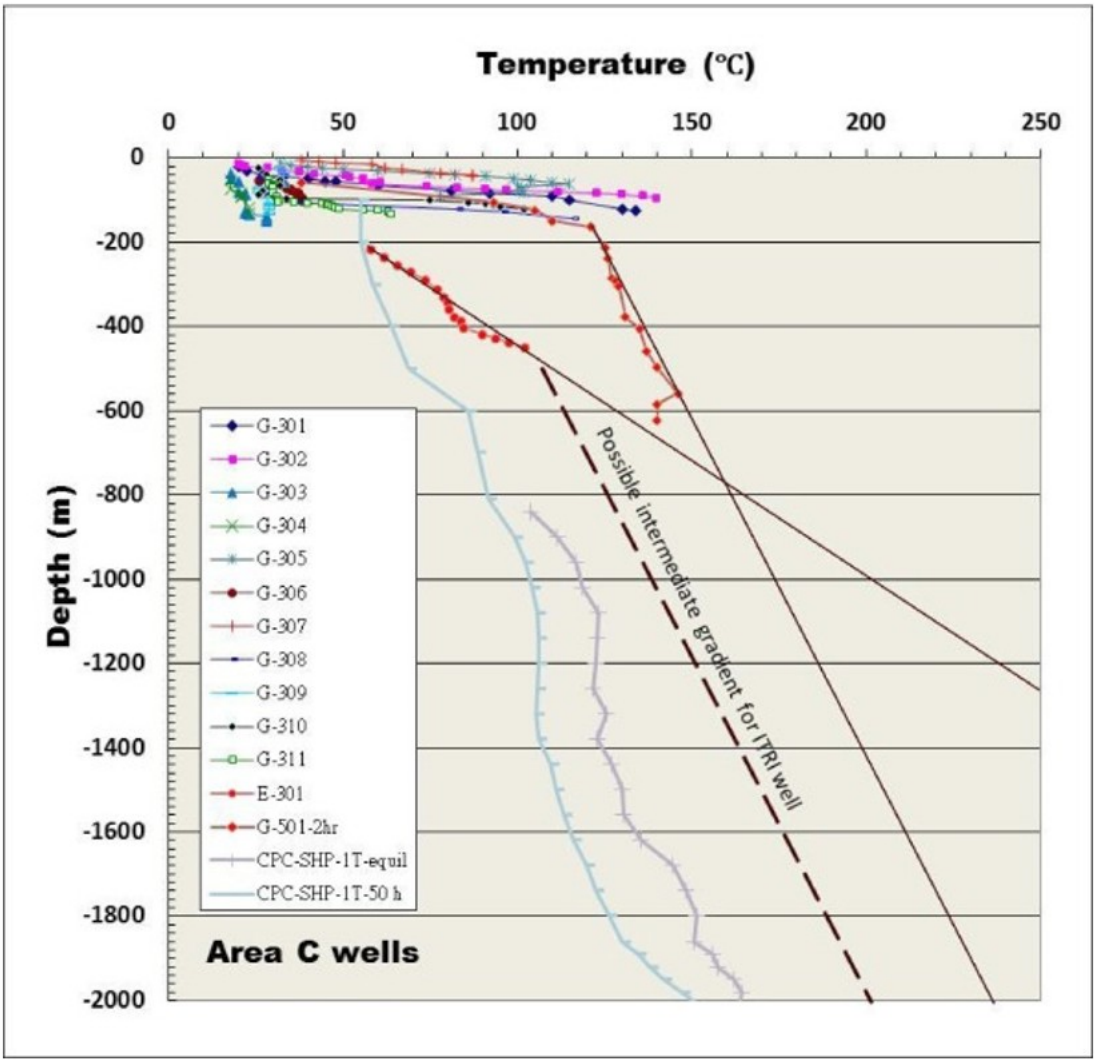

Fig. 32. Temperature depth profiles for wells in Zone C. The gradient reported for G501 is based on measurements only 2 h after drilling, thus is likely lower than actual values, and significantly below fluid inclusion temperatures of 150–170 °C obtained in core from a depth of 589 m in this well. Lines extrapolate conductive gradients for the two deepest gradient wells (E301 and G501). Curves for CPC-SHP-1T indicate measured and estimated equilibrium temperatures. The dashed line indicates an estimated possible temperature profile for the ITRI exploration well, which falls between the more marginal CPC-SHP-1T well and the other temperature gradient wells.

The reporting of sandstone at depths of 719 m (416 m below sea level) and again at 811 m (508 m below sea level) in the CPC-SHP-1T well (CPC, 1976) suggests that the Quaternary volcanic section may be thinner than it is depicted in the cross section in Fig. 30, where the contact with the Miocene Wushishan Formation is at about 625 m below sea level (this would correspond to a depth of ~925 m for the CPC-SHP-1T well). If the Wushishan Formation begins at the upper sandstone contact (416 m below sea level) in the CPC well, then the top of this formation could be encountered in the ITRI exploration well at a depth of around 870 m. Given the estimated temperature-depth profile in Fig. 31, the geothermal reservoir (temperatures >150 °C) would be located within the Miocene sedimentary sequence, which may have a lower buffering capacity than the overlying feldspar-rich volcanic section. This would then pose a greater risk of having acidic fluids present. The ITRI exploration well will provide important constraints on the actual thermal profile, the location of the contact with the Miocene sediments, and whether or not acidic fluids are present at depth.

6. Conclusions

In this study, a variety of geochemical and geophysical data from both historical and new investigations were analyzed to develop an updated conceptual model of the Tatun geothermal system. The main objective of this investigation was to evaluate the geothermal resource potential of this area, with a focus on its NE margins, which showed some likelihood of hosting thermal waters of neutral character (but of lower temperatures) as opposed to more acidic and corrosive fluids found closer to the main volcanic centers. These investigations included a geochemical and geothermometry study of water and gas chemical compositions, analyses of new magnetotelluric data to infer resistivity and presence of clay layers that could serve as a good geothermal system cap, and associated GIS and 3-D modeling that integrates all available data.

This effort suggests that the NE marginal portion of the Tatun volcanic area system may be amenable to geothermal exploitation. However, there are two important mitigating factors that need to be considered prior to making any new resource evaluations for this area. The first is to confirm whether or not there are near-neutral fluids present in portions of the deep reservoir, and how much of the reservoir contains these fluids. In geothermal systems that have both acidic and near-neutral geothermal fluids such as Biliran (Ramos-Candelaria et al., 1995; Apuada et al., 2010) and Alto Peak (Reyes et al., 1993) in the Philippines, the systems are characterized by vapor chimneys with acid fluids, surrounded and/or underlain by liquid-dominated zones where fluids have been neutralized by water-rock interaction. At Mt. Apo (also in the Philippines), the water chemistry over time in several wells has evolved to more acidic fluids, thus suggesting that the host rocks have a limited buffering capacity for acidic fluids (Rosell et al., 2015); this could also be a result of fluid drawdown caused by geothermal production. The DYK area of Tatun has clear geochemical indications of

acidic fluids, and thus only a portion of the Tatun reservoir is likely to contain near-neutral fluids that can be used for geothermal power generation. Until the presence and distribution of these fluids has been confirmed by drilling, making estimates of sustained power production at Tatun will be difficult.

Acknowledgments

This work is dedicated to the memory of Prof. Frank Yang, whose group conducted the fundamental work on gas geochemistry at Tatun. We thank Carolyn Cantwell (UC Davis) for her contributions to the study of analog acid geothermal systems. We greatly appreciate the participation of many scientists at ITRI in conducting this collaborative project, including Bo-Heng Lee, Ching-Ray Lee, Yin-Lung Han, Chun-Yang Yen, Yen-Che Liao, Lun-Tao Tong, Shoung Ouyang, Henry Li, and Pei-Shan Hsieh − their efforts were instrumental to completing this study. We also thank Prof. Ching-Ying Lan of Academia Sinica for providing us with core samples from the MSRO G-501 well, and Dr. Hsiao-Fen Lee of the Taiwan Volcano Observatory at Tatun for generously sharing her insights on the gas geochemistry of the Tatun system. Dr. Nick Mortimer of GNS Science was able to track down thin sections for samples that had been collected from Tatun over 40 years ago and provided us with his expert petrographic descriptions – we greatly appreciate his assistance. We thank Andrew Rae and Bill Cumming for their insightful and constructive reviews. Funding for this work was provided by the Industrial Technology Research Institute under contract number WF10910, as part of Work for Others funding from Berkeley Lab, provided by the Director, Office of Science, of the U.S. Department of Energy under Contract No. DE-AC02-05CH11231.

References

Apuada et al., 2010

N.A. Apuada, G.F. Sigurjonsson, A.F. Oanes**Evaluation of the hydrothermal system of Biliran Island, Philippines**

Proceedings, World Geothermal Congress 2010, Bali, Indonesia, 25–29 April, (2010), p. 4

Belousov et al., 2010

A. Belousov, M. Belousova, C.H. Chen, G.F.Zellmer**Deposits, character and timing of recent eruptions and gravitational collapses in Tatun volcanic group, northern Taiwan: hazard-related issues**

J. Volcanol. Geotherm. Res., 191 (2010), pp. 205-221

Chen and Wu, 1971

C.H. Chen, Y.J. Wu**Volcanic geology of the Tatun geothermal area, northern Taiwan**

Proceedings of the Geological Society of China, No. 14 (1971), pp. 5-20

Chen and Yang, 1984

C.H. Chen, H.Y. Yang**Mineral paragenesis in the hydrothermal alteration of andesites, as exemplified by a geothermal well in the Tatun volcanic area, northern Taiwan**

Proceedings of the Geological Society of China, No. 27 (1984), pp. 68-85

Chen et al., 2010

C.H. Chen, G.S. Burr, S.B. Lin**Time of a near Holocene volcanic eruption in the Tatun volcano group, Northern Taiwan: evidence from AMS radiocarbon dating of charcoal ash from sediments of the Sungshan Formation in Taipei Basin**

Terr. Atmos. Ocean. Sci., 21 (2010), pp. 611-614

Chen, 1970

C.H. Chen**Geology and geothermal power potential of the Tatun volcanic region**

Geothermics (1970), pp. 1134-1143

Special Issue 2

Chen, 1975

C.H. Chen**Thermal waters in Taiwan**

A Preliminary Study Proceedings of the Grenoble Symposium, August 1975, International Association of Hydrological Sciences(1975), pp. 79-88

Publication no. 119

Cheng et al., 2010

C.T. Cheng, C.T. Lee, P.S. Lin, B.S. Lin, Y.B. Tsai, S.J. Chiou**Probabalistic earthquake hazard in Metropolitan Taipei and its surrounding regions**

Terr. Atmos. Ocean. Sci., 21 (2010), pp. 429-446

CPC, 1976

Chinese Petroleum Corporation (CPC)**Weekly Geological Report of Well Sample, CPC-SHP-1T Well. Unpublished Report**

Geothermal Department, Taiwan Petroleum Exploration Division, Chinese Petroleum Corporation (1976)

Cumming, 2016

W. Cumming**Resource conceptual models of volcano-hosted geothermal reservoirs for exploration well targeting and resource capacity assessment: construction, pitfalls and challenges**

Geother. Resour. Counc. Trans., 40 (2016), pp. 623-637

D’Amore et al., 1999

F. D’Amore, A.H. Truesdell, J.R. Haizlip**Acidic geothermal fluids containing hydrochloric acid: a review**

Proceedings, 20th Annual PNOC-EDC Geothermal Conference(1999), pp. 61-72

Ellis and Giggenbach, 1971

A.J. Ellis, W. Giggenbach**Hydrogen sulphide ionization and sulpher hydrolosis in high temperature solution**

Geochim. Cosmochim. Acta, 35 (1971), pp. 247-260

Ellis, 1973

A.J. Ellis**Tatun Geothermal Region, Taiwan – the Geothermal Field, Tatun, Taiwan**

New Zealand Geochemical Group Newsletter (1973), pp. 76-77

November 1973, no. 32

Feng and Huang, 1970

T.T. Feng, K.K. Huang**Exploration of geothermal resources in the Tatun volcanic region, Taiwan, Republic of China**

Geothermics (1970), pp. 150-154

Special Issue 2

Fournier and Thompson, 1993

R.O. Fournier, J.M. Thompson**Composition of steam in the system NaCl-KCl-H_2O-quartz at 600 °C**

Geochim. Cosmochim. Acta, 57 (1993), pp. 4365-4375

Gasperikova et al., 2015

E. Gasperikova, G.K. Rosenkjaer, K. Arnason, G.A. Newman, N.J. Lindsey**Resistivity characterization of the Krafla and Hengill geothermal fields through 3D MT inverse modeling**

Geothermics, 57 (2015), pp. 246-257

Giggenbach, 1981

W.F. Giggenbach**Geothermal mineral equilibria**

Geochim. Cosmochim. Acta, 45 (1981), pp. 393-410

Giggenbach, 1987

W.F. Giggenbach**Redox processes governing the chemistry of fumarolic gas discharges from White Island, New Zealand**

Appl. Geochem., 2 (1987), pp. 143-161

Giggenbach, 1988

W.F. Giggenbach**Geothermal solute equilibria: derivation of Na-K-Mg-Ca geoindicators**

Geochim. Cosmochim. Acta, 52 (1988), pp. 2749-2765

Giggenbach, 1991

W.F. Giggenbach**Chemical techniques in geothermal exploration**

Applications of Geochemistry in Geothermal Reservoir Development, F. D'Amore (coordinator), United Nations Institute for Training and Research (1991), pp. 119-144

Giggenbach, 1992

W.F. Giggenbach**Isotopic shifts in waters from geothermal and volcanic systems along convergent plate boundaries and their origins**

Earth Planet. Sci. Lett., 113 (1992), pp. 495-510

Giggenbach, 1997

W.F. Giggenbach**The origin and evolution of fluids in magmatic-hydrothermal systems**

H.L. Barnes (Ed.), Geochemistry of Hydrothermal Ore Deposits(3rd Edition), John Wiley and Sons (1997), pp. 737-796

Komori et al., 2014

S. Komori, M. Utsugi, T. Kagiyama, H. Inoue, C.-H.Chen, H.-T. Chiang, B.F. Chao, R. Yoshimura, W. Kanda**Hydrothermal system in the Tatun Volcano Group, northern Taiwan, inferred from crustal resistivity structure by audio-magnetotellurics**

Prog. Earth Planet. Sci., 2014 (1) (2014), p. 20

Konstantinou et al., 2009

K.I. Konstantinou, C.H. Lin, W.T. Liang, Y.C.Chan**Seismogenic stress field beneath the Tatun Volcano Group, northern Taiwan**

J. Volcanol. Geotherm. Res., 187 (2009), pp. 261-271

Lan et al., 1980

C.Y. Lan, J.G. Liou, Y. Seki**Investigation of drillhole core samples from Tatun geothermal area, Taiwan**

Proceedings, 3rd International Symposium on Water-Rock Interaction, Edmonton, Canada (1980), pp. 183-185

Lee et al., 1994

C.R. Lee, D.Y. Chiang, R.H. Chen**Compilation of the Geothermal Prospects Data in Taiwan During 1966–1979. Bureau of Energy Report**

(1994), p. 500

in Chinese

Lee et al., 2005

H.F. Lee, T.F. Yang, T.F. Lan**Fumarolic gas composition of the Tatun volcano group, Northern Taiwan**

Terr. Atmos. Ocean. Sci., 16 (2005), pp. 843-864

Lee et al., 2008

H.F. Lee, T.F. Yang, T.F. Lan, C.H. Chen, S.R. Song, S.Tsao**Temporal variations of gas compositions of fumaroles in the Tatun volcano group, northern Taiwan**

J. Volcanol. Geotherm. Res., 178 (2008), pp. 624-635

Lindsey and Newman, 2015

N. Lindsey, G. Newman**Improved workflow for 3D inverse modeling of magnetotelluric data: examples from five geothermal systems**

Geothermics, 53 (2015), pp. 527-532

Liu et al., 2011

C.M. Liu, S.R. Song, Y.L. Chen, S. Tsao**Characteristics and origins of hot springs in the Tatun Volcano Group in northern Taiwan**

Terr. Atmos. Ocean. Sci., 22 (2011), pp. 475-489

MRSO, 1969

MRSO**The Report on Geothermal Exploration of Tatun Volcano Group I**

Mineral Research and Service Organization (1969)

Report 90

MRSO, 1970a

MRSO**The Report on Geothermal Exploration of Tatun Volcano Group II**

Mineral Research and Service Organization (1970)

Report 102

MRSO, 1970b

MRSO**Assembled Reports by Foreign Experts in Geothermal Investigation I**

Mineral Research and Service Organization (1970)

Report 105

MRSO, 1971

MRSO**Letter and blue print from Mao-Hwa Po, President, to Donald E. White, dated March 26, 1971, summarizing flowing pressure and pH data for wells MW-205 and MW-208**

Mining Research and Service Organization (1971)

MRSO PG 60-13

MRSO, 1973a

MRSO**The Report on Geothermal Exploration of Tatun Volcano Group IV**

Mineral Research and Service Organization (1973)

Report 126

MRSO, 1973b

MRSO**Assembled Reports by Foreign Experts in Geothermal Investigation II**

Mineral Research and Service Organization (1973)

Report 127

Newman and Alumbaugh, 2000

G.A. Newman, D.L. Alumbaugh**Three-dimensional magnetotelluric inversion using non-linear conjugate gradients**

Geophys. J. Int., 140 (2000), pp. 410-424

Newman and Boggs, 2004

G.A. Newman, P.T. Boggs**Solution accelerators for large-scale three-dimensional electromagnetic inverse problems**

Inverse Prob., 20 (2004), pp. S151-S170

Newman et al., 2003

G.A. Newman, S. Recher, B. Tezkan, F.M.Neubauer**3-D inversion of a scalar radio magnetotelluric field data set**

Geophysics, 68 (2003), pp. 782-790

Ohba et al., 2010

T. Ohba, T. Sawa, N. Taira, T.F. Yang, H.F. Lee, T.F.Lan, M. Ohwada, N. Morikawa, K. Kazahaya**Magmatic fluids of Tatun volcanic group, Taiwan**

Appl. Geochem., 25 (2010), pp. 513-523

Ohsawa et al., 2013

S. Ohsawa, H.F. Lee, B. Liang, S. Komori, C.H.Chen, T. Kagiyama**Geochemical characteristics and origins of acid hot spring waters in the Tatun volcanic group, Taiwan**

J. Hot Spring Sci., 62 (2013), pp. 282-293

Powell and Cumming, 2010

T. Powell, W. Cumming**Spreadsheets for geothermal water and gas geochemistry**

Proceedings, 35th Workshop on Geothermal Reservoir Engineering, Stanford University, Stanford, CA (2010)

SGP –TR-188

Ramos-Candelaria et al., 1995

M. Ramos-Candelaria, D.R. Sanchez, N.D. Salonga**Magmatic contributions to Philippine hydrothermal systems**

Proceedings, World Geothermal Congress 1995, Florence, Italy(1995), pp. 1337-1341

Reyes et al., 1993

A.G. Reyes, W.F. Giggenbach, J.R.M. Saleras, N.D.Salonga, M.C. Vergara**Petrology and geochemistry of Alto Peak a vapor-cored hydrothermal system, Leyte Province, Philippines**

Geothermics, 22 (1993), pp. 479-519

Rosell et al., 2015

J.B. Rosell, R.J.T. Tamboboy, B.G. Sambrano, D.B.Dacillo, M.H. Reed**Mt. Apo acid fluid evolution: exploring the role of rock buffers in the reservoir pH changes with time**

Proceedings, World Geothermal Congress 2015, Melbourne, Australia, 19–25 April (2015), p. 7

Siripunvaraporn and Egbert, 2009

W. Siripunvaraporn, G. Egbert**WSINV3DMT: vertical magnetic field transfer function inversion and parallel implementation**

Phys. Earth Planet. Inter., 173 (2009), pp. 317-329

Siripunvaraporn et al., 2005

W. Siripunvaraporn, G. Egbert, Y. Lenbury, M. Uyeshima**Three-dimensional magnetotelluric inversion: data-space method**

Phys. Earth Planet. Inter., 150 (2005), pp. 3-14

Siripunvaraporn, 2011

W. Siripunvaraporn**Three-dimensional magnetotelluric inversion: an introductory guide for developers and users**

Surv. Geophys., 33 (2011), pp. 5-27

Song et al., 2000

S.R. Song, S. Tsao, H.J. Lo**Characteristics of the Tatun volcanic eruptions, north Taiwan: implications for a cauldron formation and volcanic evolution**

J. Geol. Soc. China, 43 (2000), pp. 361-378

Tamboboy et al., 2015

R.J.T. Tamboboy, G.M. Aragon, M.H. Reed**Evaluation of NaOH injection in the neutralization of highly acidic Cl-SO_4 and SiO_2-saturated geothermal fluids**

Proceedings, World Geothermal Congress 2015, Melbourne, Australia, 19–25 April (2015), p. 8

Truesdell et al., 1989

A.H. Truesdell, J.R. Haizlip, H. Armannsson, F.D'Amore**Origin and transport of chloride in superheated geothermal steam**

Geothermics, 18 (1989), pp. 295-304

Truesdell, 1991

A.H. Truesdell**Origins of acid fluids in geothermal reservoirs**

Geother. Resour. Counc. Trans., 15 (1991), pp. 289-296

Truesdell, 2000

A.H. Truesdell**Sulfate in active geothermal systems from source to surface**

Geol. Soc. Am. Abstr. Program., 32 (2000), pp. A-49

n. 7

Tsai et al., 2010

Y.W. Tsai, S.R. Song, H.F. Chen, S.F. Li, C.H. Lo, W. Lo, S. Tsao**Volcanic stratigraphy and potential hazards of the Chihsingshan volcano subgroup in the Tatun volcano group, Northern Taiwan**

Terr. Atmos. Ocean. Sci., 21 (2010), pp. 587-598

Ussher et al., 2000

G. Ussher, C. Harvey, R. Johnstone, E. Anderson**Understanding the resistivities observed in geothermal systems**

Proceedings, World Geothermal Congress 2000, Kyushu-Tohoku, Japan, May 28–June 10 (2000), pp. 1915-1920

Vidal, 1999

B.C. Vidal**The origin and mechanism of the acidic discharge of production well BL1D, Southern Negros Geothermal Field, Central Philippines**

Proceedings of the 20th Annual PNOC-EDC Geothermal Conference, Makati City, Philippines, March 4&5 (1999), pp. 37-45

Wang et al., 1999

K.L. Wang, S.L. Chung, C.H. Chen, R. Shinjo, T.F.Yang, C.H. Chen**Post-collisional magmatism around northern Taiwan and its relation with opening of the Okinawa Trough**

Tectonophysics, 308 (1999), pp. 363-376

Witt et al., 2008

M.L.I. Witt, T.P. Fischer, D.M. Pyle, T.F. Yang, G.F.Zellmer**Fumarole compositions and mercury emissions from the Tatun Volcanic Field, Taiwan: results from multi-component gas analyser, portable mercury spectrometer and direct sampling techniques**

J. Volcanol. Geotherm. Res., 178 (2008), pp. 636-643

Yang et al., 1999

T.F. Yang, Y. Sano, S.R. Song**^{3}He/^{4}He Ratios of Fumaroles and Bubbling Gases of Hot Springs in Tatun Volcano Group, North Taiwan. Il Nuovo Cimento 22C**

(1999), pp. 281-286

Yen et al., 1984

T.P. Yen, Y.-H. Tzou, W.-H. Lin**Subsurface Geology of the Region of the Tatun Volcano Group. Petroleum Geology of Taiwan, No. 20**

(1984), pp. 143-154

Zhang et al., 2009

G. Zhang, N. Spycher, E. Sonnenthal, C. Steefel**Modeling acid-gas generation from boiling chloride brines**

Geochem. Trans., 2009 (10) (2009), p. 11, 10.1186/1467-4866-10-11

[1] Now at Department of Earth and Planetary Science, University of California, Berkeley, Berkeley, CA, USA.

[2] Now at Department of Earth Sciences, University of Minnesota, Minneapolis, MN 55455, USA.